RESOURCE GEOLOGY, vol. 56, no. 3, 293–314, 2006

Element Mobility in Melts during Successive Intrusions of Crustal-derived Magmas and Sn-W Mineralization

Jean-Louis VIGNERESSE

Nancy-Universités, CREGU, UMR CNRS 7566 G2R, BP 23, F-54501 Vandoeuvre Cedex, France
[e-mail: jean-louis.vigneresse@g2r.uhp-nancy.fr]
Received on March 27, 2006; accepted on June 22, 2006

Abstract: Continental collisions are the place where granitic plutons result from the melting of crustal components. Granitic plutons are built up by successive input of magma with a variable composition and hence temperature and chemistry. The intrusion of a new magma batch has consequences on the element mobility in the melt. Diffusion in already formed crystals is limited, due to the short time interval between magma input, and because of the low values of element diffusivity in solids. Because the new magma is generally hotter than the magma chamber, the temperature in the contact zone is modified. It activates diffusion by and modifies its characteristic length for element mobility in the melt. A new intrusion also modifies the partition coefficients, decreasing compatibility and increasing the incompatibility. The change in temperature has also effects on fluid exsolution controlled by crystallization, or second boiling. The present paper examines the intrusion of magma (felsic or mafic) into a felsic magma chamber with a time interval of 30 ky. The intrusion of magma with similar composition, hence low (±100°C) temperature difference has few effects. The diffusion lengths for elements rarely exceed one order of magnitude. The fluids released by the cooling magma are balanced by their reincorporation into the warming magma. In contrast, the intrusion of mafic magma into felsic magma chamber results in temperature difference that can reach ±300°C. It may change the diffusion length up to two orders of magnitude for elements having large activation energy. Partition coefficients also vary by more than one order of magnitude. The effect is enhanced in the warming felsic magma, and damped in the mafic magma. In consequence elements like As, Sn, Sr, W, Zr are driven from the mafic magma toward the felsic magma. The release of H_2O and CO_2 are balanced between the two magma types. However the mafic magma releases an important amount of S that cannot re-dissolves into the felsic magma and remains in the fluid phase. This simple model also addresses processes acting during ore formation. In particular, it examines the behavior of ions with a four valences state, as Sn and W, which has implications on the incorporation of other elements sharing a similar structure. It points out the necessity of external factors (S, halogens content and redox conditions) for controlling ore formation.

Keywords: granite emplacement, diffusion, mineralization, degassing

1. Introduction

Base metals (Sn-W) deposits linked to felsic magmas are commonly associated with reduced granitic plutons often within settings of continental collision. The mineral composition, the low oxidation state of the magma and the occurrence of numerous crustal blocks with roof pendants indicate a strong crustal component. The restricted circulation of hydrothermal fluids immediately associated to magma emplacement and the development of strong fluid circulation while magma is nearly crystallized indicate strong fluid-rocks interactions delayed after emplacement. This situation strongly contrasts with porphyry-type Cu-Mo ore deposits, in which mineralization is intimately associated with magma emplacement. For example, detailed studies of Sn and W mineralizations of the Cornubian batholith, SW England, indicate diachronous and independent histories of magmatism with ages ranging from 293 to 274 Ma (Darbyshire and Shepherd, 1994) and mineralization dated around 286 Ma, 2 or 3 My after cooling of the closest pluton (Chen et al., 1993), and associated with fluid circulation (Gleeson et al., 2001). Similarly, the Mole granite, NSW Australia, shows a compositional evolution of the fluid phase associated to ore deposits (Sn-W-F) over a wide range of temperature from 600 to 300°C (Pettke et al., 2005), that is well below magma mobility as a whole. This event occurred over 4 My after first magma settling (Schaltegger et al., 2005), which leaves abundant time for the magma to cool down and crystallize.

In the two above examples, the granitic magmas present all characters of crustal-derived magmas. The Mole granite is a highly fractionated granite within the New England Batholith, in which the silica content ranges from 47 to 79 % (Blevin et al., 1996). Similarly in the Erzgebirge Sn-W ore Province, Germany, the silica content ranges from 62 to 77 % (Breiter et al., 1999; Förster et al., 1999). In the case of the Erzgebirge, about 14 magmatic phases have been identified, ranging from rhyolites to microgranite (Müller et al., 2005) documenting magma mixing. The New England Batholith consists of intrusive

rocks ranging from monzogranites and granodiorites to minor tonalites, diorites and gabbros, but also some large, highly-fractionated granites (Shaw and Flood, 1981). Such a range of silica variation, either within a single massif, or at a province scale, does not show evidence of alkaline depletion resulting from late hydrothermal alteration. It has been interpreted as the result of extreme differentiation of the magma (Blevin, 2004). Such magmas present low oxidation character marked by Fe_2O_3/FeO commonly lower than 0.1 and high Rb/Sr ratio (10-100).

Detailed field observations document a different story. Most of those plutons show evidence of multiple magma intrusions. A complex history of intrusions is manifested in the Erzgebirge, where several mineralogical facies are found with interactions between them, depending on the rheological stage to which they intruded a former emplaced magma (Seltmann and Farragher, 1994). Hence, early high temperature Sn-W deposits are associated with the emplacement of highly evolved granitic melts, often rich in volatiles (Tischendorf, 1988; Stemprok, 1993). More generally, granitic plutons are presently considered as the result of successive magma inputs with different chemical composition (Pitcher and Hutton, 1982; Glazner et al., 2004; Vigneresse, 2004). The ubiquitous observation of different rock types that form any granitic pluton also indicates that the chemistry of those magmas has varied with time. In all observed cases, a complex interaction took place between the successive pulses of magma, their fluid content and the surrounding rocks.

The preceding examples point to a discontinuous timing of the successive magmatic events leading to Sn-W ore generation. Though discontinuous magma inputs have already been addressed for pluton building (Pitcher and Hutton, 1982; Guillet et al., 1985), their effects have rarely been considered for their implications during ore genesis.

The present paper examines the consequence of successive magma intrusion on the parameters controlling element mobility in magmas. Hence, if a pluton is built from the succession of several magma inputs with different temperature and composition, the intrusion of a new magma should modify the element mobility, including fluids. In a first order treatment, magma advection is considered as instantaneous and element mobility is attributed to diffusion. Generalized diffusion is inspected through a characteristic length, the length along which an element diffuses in a given period of time (Crank, 1975). It serves as a basis to determine the respective influence of diffusion when the temperature varies. The length is computed from the diffusivity value, which has some constant value and an exponential expression for temperature (Jambon, 1982). The latter is controlled by the activation energy of the element. The value of the partition coefficients determines the ability of an element to combine and to enter within the crystallographic network of a given minerals phase. It is a specific case of diffusion. The nature and importance of the fluid phase is also examined.

2. Melting and Ascent Conditions for the Magma

Granitic magmas form by melting of the intermediate to lower crust, under heat sources generally controlled by the mantle activity. Water is essential to induce crustal melting and to rule melt mobility. However, the difficulty to introduce free water down to the lower crust, joint with the dry character of granulitic rocks, clearly limit the efficiency of the reaction for generating large volumes of hydrated granitic melts. Nevertheless, it can give place to migmatites and anatectic granites (Mehnert, 1968). A second possibility consists in the breakdown of hydrous minerals, as micas and amphiboles. The reactions liberate OH^- radicals that are immediately reincorporated to the melt. The residual mineral phase left by the breakdown reactions is similar to that observed in granulitic rocks (Thompson, 1982; Clemens, 1990). Minerals involved in crustal-derived magmas essentially result from the breakdown of muscovite and biotite.

2.1. Melting conditions

Melting starts with muscovite dehydration at about 700°C (Fig. 1), and it ends at about 780°C (Harris et al., 1995). The amount of melt requires about the same quantity of muscovite and about one third of quartz and plagioclase in equal quantity to each other (Patiño Douce and Harris, 1998). Water naturally enhances the reaction since it produces a double volume of melt compared to that produced in dry conditions. In this case, the amount of plagioclase should be the double to that of quartz (Patiño Douce and Johnston, 1991). However, the quantity of melt remains low due to the limited amount of muscovite in crustal rocks.

Biotite starts melting at higher temperatures, from 780 to 870°C (Fig. 1). About two third of quartz and plagioclase and one volume of biotite, produce a slightly larger amount of melt (Patiño Douce and Beard, 1995). The residual phase includes K-feldspar and orthopyroxene or garnet. Free water also enhances melt production whereas pressure shifts the reaction to higher temperature (Patiño Douce and Beard, 1995). During the reaction, the remaining biotite becomes richer in magnesium (Icenhower and London, 1995) and it can be considered as the main source for Fe, Mn, Rb and Cs in the melt. The resulting felsic melt is mostly peraluminous, with a K/Na ratio larger than unity (Whitney, 1990).

Obviously, the temperature interval for micas breakdown ranges in the low range within the bulk solidus-liquidus interval for granite melting, giving place to "cold" magmas (Chappell et al., 1998). Hence, the bulk low

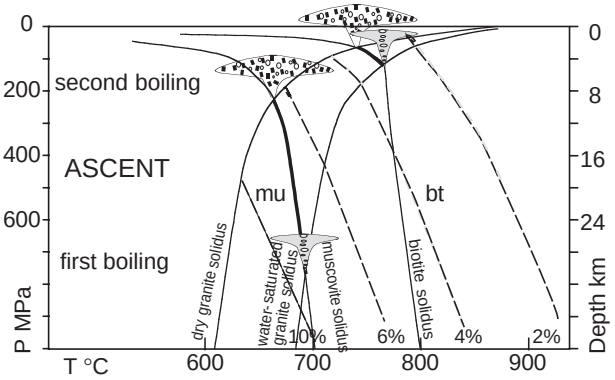

Fig. 1 PT conditions for muscovite-biotite- and biotite-bearing granitic magmas. Relative positions of fluid exsolution, second and first boiling, are indicated. Also indicated the saturation curves for water in vol %, marked in grey. The path along which first boiling occurs, due to magma decompression, is highlighted. In consequence the nature of the magma that is finally emplaced at different depth levels has not the same fluid content.

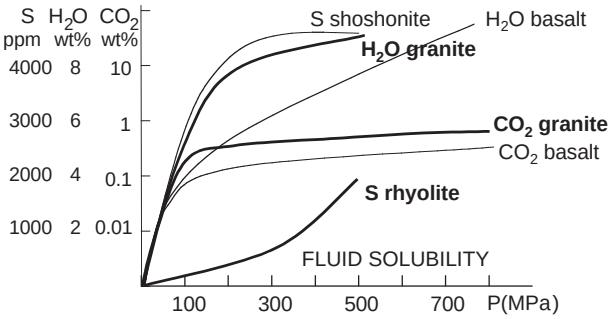

Fig. 2 Fluid solubility as a function of pressure. H_2O and CO_2 curves are from Holtz et al. (1996) and the S curves from Wallace (2001, 2005). Thick curves are for felsic magma whereas thin ones are for a basaltic composition. Note that the scales are in logarithmic scale only for CO_2 and normal scale for H_2O and S. H_2O and CO_2 contents have a similar path for both compositions, and thus a common behavior, certainly different on the exact volume of involved fluid. Conversely, S presents a contrasted evolution in both types of magma.

melting grade associated to those magmas implies that the melt contains restitic minerals and inherited zircons entrained in the melt (Miller et al., 2003). By opposition, "hot" magmas result from a higher degree of melting and consequently present populations with less inherited zircons.

2.2. Fluid content

The discrepancy between hot and cold granites has also consequences on their initial water content, hence on the quantity of fluids they can release during the ascent and emplacement.

The presence of H_2O in the melt dramatically lowers the solidus. This is valid for melts, but also for melting curves of individual minerals. Indeed the fluid saturated melting curve of albite (Knoche et al., 1992) is about 400°C lower than the dry melting curve at about 500 MPa (Boyd and England, 1963). In addition, the saturated curve always presents a negative slope in a pressure-temperature diagram, and this slope is more pronounced in the low pressure range. The initial water solubility therefore controls the temperature of intersection with the solidus curve, and thus the pressure, or minimum depth to which magma can rise (Fig. 1). This has been measured (Johannes and Holtz, 1996) for several magma compositions (Fig. 2) presenting different values of ANK, the ratio Al/(Na + K). At 500 MPa, water solubility goes through a minimum at 9 % wt for meta-aluminous granites (with ANK = 1), decreasing from 10 % wt in peraluminous melts (ANK > 1), before increasing to 12 % wt when ANK = 0.6 corresponding to peralkaline melts (Behrens and Jantos, 2001).

The incorporation of water in a granitic melt has also control on the level to which magma can ascend in the crust. Magma is mobile up to intersect the solidus curve. Therefore, a granitic magma cannot be saturated at the source, otherwise it would crystallize as soon it begins ascending toward lower pressures (Cann, 1970). A magma nearly saturated in water has great difficulties to move upward. However, a second effect develops related to the ascent and starting of crystallization. With the ascent, i.e. pressure decrease, water solubility also decreases. The ascending magma progressively exsolves its fluid phase during first boiling (Candela, 1997). A second stage of fluid release, or second boiling, (Fig. 1) occurs during crystallization. While melt shrinks, water concentration in the melt increases until saturation, becomes incompatible and exsolves. Nevertheless, the terms “first” and “second" boiling do not imply any order for these events to occur (Cline, 2003).

Considering a muscovite-bearing magma with about 8 % water at the source, it starts crystallizing between 18 and 7 km in depth (Fig. 1). In that interval, the solubility decreases by about 2 % (Fig. 2) corresponding to first boiling. Crystallization develops while magma is still mobile, so first and second boilings are coeval.

Biotite-bearing magmas are able to reach higher crustal levels (Fig. 1). A magma with 5 % water initially intersects the saturated solidus curve at 50 MPa, or 4 km. Water solubility is still 3 % at that depth, so only 2 % water is exsolved during first boiling. Along the same depth interval, a basaltic magma exsolves about 5 of its initial 8 % water (Fig. 2). Those events are controlled by the pressure loss, thus by the magma ascent velocity. According to the strain rate commonly developing during magma ascent, for which a value of 10^{-12} s^{-1} has been estimated (Harris et al., 2000), the fluid is slowly released.

2.3. Viscosity conditions

The temperature condition and the composition of magma during and after intrusion are simplified since only

first order effects are considered. First, a felsic granite and a mafic basalt constitute the two end-members magmas. Their initial temperatures are 800°C for the granite and 1200°C for the basalt. Second, the new incoming magma is taken as a viscous magma, nearly free of solid phase as first forming crystals or restitic bodies, and it presents the viscosity of the pure melt. The viscosity of the mafic magma is assigned to 10 Pa.s (Giordano and Dingwell, 2003), whereas the granitic melt presents a viscosity of 10^6 Pa.s (Clemens and Petford, 1999).

Third, the yet emplaced magma had started to crystallize, but it has not yet reached total solidification, assuming a temperature 200°C lower than the liquidus. The percentage of formed crystals is assumed to be less than 50 %, the value for rigidity onset in the framework formed by the crystal suspension (Vigneresse et al., 1996). The selected value of crystallinity is 33 % for simplicity. The relative viscosity (η/η_0) can be computed, using the Einstein Roscoe equation (Einstein, 1906; Roscoe, 1952). For dilute suspensions, it is a power law that relates the relative viscosity to the crystal percentage (Φ) with a coefficient (n = 2.5). At higher crystal percentage, it has been modified (Krieger and Dougherty, 1959) by introducing the maximum package (Φ_{max}) value within the power coefficient resulting in a new coefficient (m = n Φ_{max}) :

$$\eta = \eta_0 (1 - \Phi/\Phi_{max})^{-m} \quad (1)$$

Assuming a value of Φ/Φ_{max} = 0.33/0.75 and a coefficient m equal to 1.8 (Vigneresse and Burg, 2004), the change in viscosity is restricted to less than one order of magnitude.

The viscosity change due to temperature variation follows an Arrhenius law, in which the activation energy is around 300 kJ/mole (Maaløe, 1985). The increase is by 1 order of magnitude between 1200 and 1000°C, then only 2 between 1000 and 800°C and finally 3 orders of magnitude between 800 and 600°C.

3. Time Scale

The time period for the successive magma inputs to be amalgamated into a single pluton is given by dating. An upper limit for pluton formation is of the order of 2 My (Petford et al., 2000), resulting from a succession of some tens of magma pulses. This provides an estimate for the time of emplacement, between 10 and 100 ky. Precise dating realized on mineralized porphyry-type deposits also indicate such time period, with a resolution of some tens of ky (Stein et al., 2001).

Another method of estimating the interval between magma pulses is provided by computation on melt segregation. Indeed, the time needed to segregate melt from its source region controls the time interval for emplacement (Rabinowicz and Vigneresse, 2004). If too much melt is produced, the matrix becomes too soft and cannot expel melt any more. If melting cannot afford melt in enough quantity, the source becomes stiff and segregation stops. A window of 5-10 % melt is required that leads to successive periods of melting and segregation (Rabinowicz and Vigneresse, 2004). The time to produce this amount of melt is about 30 ky. From both methods, an average of 30 ky is adopted for the time interval between two magma inputs.

4. Generalized Diffusion

Heat and element diffusions are commonly addressed through diffusive equations (Crank, 1975). Melt motion within its matrix is a specific case of flow in a porous medium. It follows a modified Navier-Stokes equation, which corresponds to the diffusion of momentum, product of the mass by its velocity. The similarity of transport equations, which are all diffusive, has been known for a long time, and proceeds from the electronic properties of crystals. The Nernst-Einstein equation relates electrical conductivity to diffusivity and the Stokes-Einstein equation relates viscosity to diffusivity (Magaritz and Hofmann, 1978). In silicates melts, the Eyring equation, relating viscosity to diffusivity, is of practical use (Mysen, 1998). The relationship between elastic properties and partition coefficient follows from a similar process (Blundy and Wood, 2003). Those equations may be compared together, predicting the range of instabilities development, but the form of those instabilities is by nature less predictable.

The progressive return from randomly concentrated elements to an averaged distribution occurs through diffusion. It aims to smooth the concentration gradient, thus decreasing the free energy of the system (Carlslaw and Jaeger, 1959; Crank, 1975). A stationary diffusion law describes the flux of matter, relating the flux to the gradient through a diffusion coefficient. For element diffusion in a solid or in a melt, it is the usual diffusion coefficient (D_s or D_m). For heat it is the thermal diffusivity (D_h), and for a viscous flow, it is a combination of viscosity (η) and density (ρ), leading to an effective viscosity (ν).

4.1. Heat diffusion

In such situations, a differential equation relates the variation of temperature (T) with time (t) to the concentration gradient and to the sources (Q) (Crank, 1975).

$$\delta T/\delta t = -D_h \, \delta^2 T/\delta x^2 + Q \quad (2)$$

Adopting the thermal diffusivity (D_h), a characteristic length simply relates the time (τ) to the square of the length (L) along which the flow advances. The equation for heat diffusion writes

$$\tau = D_h^{-1} L^2 \quad (3)$$

When dealing with element diffusion, the introduction of diffusivity simplifies the Equation 2. Fick's law only states that the flux of elements with time varies according to the concentration (c) gradient, and the equation writes

$$\delta c/\delta t = -D\, \delta^2 c/\delta x^2 \quad (4)$$

A characteristic length, similar to that of temperature variation simply writes

$$\tau = D^{-1} L^2 \quad (5)$$

The solution depends on the concentration distribution within a given geometry (Crank, 1975). For the present purpose, the use of a characteristic length is preferred. It is simpler and allows direct comparisons between the several processes that develop (Fig. 3).

For heat diffusion, the thermal diffusivity (D_h) of the crust is 10^{-6} m^2/s (Richardson and Oxburgh, 1978). It depends on thermal conductivity, for which the variations with temperature, especially at high conditions (> 500°C), are not yet really determined.

4.2. Element diffusion

Values of diffusion coefficients in melts or in solids are extremely variable. They depend on the conditions of measurement, especially on the range of considered temperature and also in which mineral the element is diffusing (Brady, 1995). Other conditions as pressure and oxygen fugacity (Mungall and Dingwell, 1997) are not considered here. Commonly measured values of diffusion coefficients in solids (D_s) are in the range 10^{-10} to 10^{-22} m^2/s (Brady, 1995). In melts the values (D_m) are higher, ranging 10^{-9} to 10^{-16} m^2/s (Jambon, 1982).

Adopting the average value of 10^{-6} m^2/s for heat diffusion, a median diffusion coefficient in melts at 10^{-12} m^2/s and 10^{-18} m^2/s for diffusion in solids allows considering only one equation

$$\tau = 0.03\, L^2 \quad (6)$$

This equation scales in km/My for heat, in m/My for elements diffusion in melts, and in mm/My for element diffusion in solids (Fig. 3).

4.3. Viscosity diffusion

When dealing with viscosity diffusion, the dynamic viscosity ($\nu = \eta/\rho$) has the dimension of diffusivity (m^2/s), but it cannot be used directly to compute motion of the viscous phase. Hence, the Navier-Stokes equation that rules viscous flow is the equation of momentum diffusion, but it does not scale the velocity itself. The product of the velocity (V) of the viscous body by some distance (L) scales in m^2/s and can be compared to the dynamic viscosity. The Péclet number quantifies the ratio of the momentum during advection to the momentum during diffusion (Turcotte and Schubert, 1982). When the Péclet number is larger than 1, then advection dominates over diffusion.

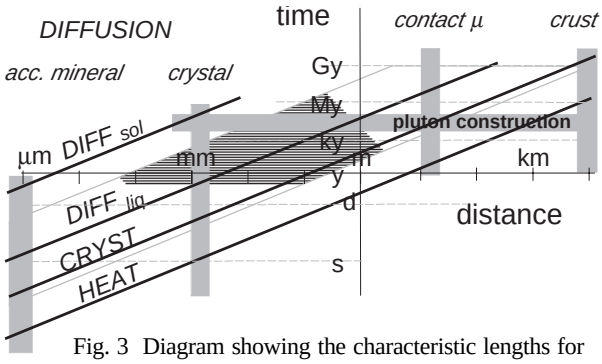

Fig. 3 Diagram showing the characteristic lengths for diffusive events. The time-scale is graduated in seconds, then in day, and usual time scale in years. Distances are graduated in a logarithmic scale, from mm to km. Average distances are indicated for accessory minerals, common crystals, contact metamorphism and crustal thermal events. The thick lines indicate the average values of element diffusion in solid and melts, magma crystallization and heat diffusion. The range of diffusion in melts is indicated by a stippled box around an average value.

$$P_e = VL/\nu \quad (7)$$

The velocity (V) represents a balance between buoyancy and viscous forces or between inertia and buoyancy forces, provided the viscous effects are small. When the balance is between viscous force and buoyancy then the scale is

$$V = (\Delta\rho/\rho)*g*L^2/\eta \quad (8)$$

In the case of magma interaction, the value of $(\Delta\rho/\rho)*g$ can be estimated as 1.0 and the time to reach the distance of diffusion at the onset of convection can be estimated as

$$\tau \sim \nu^{-1} L^2 \quad (9)$$

An equation similar to the preceding for diffusion results, giving values of 0.8 cm/y for magma of viscosity 10^0 Pa.s. It provides a maximum scale for convection of 240 m assuming duration of 30 ky. In the case of felsic magma with viscosity of 10^6 Pa.s, the scale is reduced to a boundary layer of 240 mm.

4.4. Fluid exsolution

The fluid loss during crystallization, or second boiling, is commonly linked to the rate of crystallization (Candela, 1997). According to experimental (Maaløe, 1985), numerical (Spohn et al., 1988), and quantitative textural (Cashman, 1990) studies, estimated nucleation and growth rates are approximately constant at 10^{-10} to 5×10^{-11} $cm.s^{-1}$ under most magmatic cooling conditions.

The crystallization rate $\partial\Phi/\partial t$ may be approximated as the linear variation in temperature in the interval of crystallization ΔT between the liquidus T_L and solidus T_S temperatures from which the rate of crystallization with time can be inferred

$$\Phi = (T_L - T) / (T_L - T_s) \qquad (10)$$

A second approximation considers the modified thermal diffusivity (κ') that takes into account the latent heat (L) effects

$$\kappa' = \kappa / [\rho\, c\, (1 + L / c\Delta T)] \qquad (11)$$

Given the specific heat of a magma 10^3 J/kg/K and the latent heat of crystallization at about 4×10^5 J/kg (Weinberg et al., 2001), the thermal diffusivity is lowered by a factor of 2.5, which yields a value of 4×10^{-5} m^2/s. In terms of characteristic length it results in halving the diffusion length compared to thermal diffusion. Finally, the rate of crystallization can be also be approached through a generalized diffusion of heat, that takes into accounts crystal growth, nucleation rate, thermal diffusivity and other related effects, approximating a characteristic length for crystallinity (Shinohara and Kazahaya, 1995)

$$\tau_\chi = a\, L^2 \qquad (12)$$

The constant $a^{-1/2}$ is estimated at 8×10^{-4} for a silicic magma chamber (Brandeis and Jaupart, 1987; Shinohara and Hedenquist, 1997). The constant (a) scales as 6×10^9 m^2/s in the present notation (Eq. 6). It ranges between the rate of heat diffusion and element diffusion (Fig. 3).

4.5. Partition coefficients

Partition coefficients $K^{melt/min}$ measure the preference of a chemical element from the melt to incorporate a given mineral phase. Elements with a partition coefficient K greater than 1 are said compatible within the given phase. In contrast, values lower than unity reflect the non-affinity of the incompatible element for the phase. The value of partition coefficients corresponds to the ratio of weight fraction of the element between the two phases (Rollinson, 1993; Blundy and Wood, 2003). The coefficient magnitude is controlled by the strain field and the electronic balance the element imposes to the existing atomic lattice in which it is incorporated. Thus, it basically depends on its ionic radius and its state of valence (Fig. 4). A parabolic function represents the variation of partition coefficients of elements with a given valence as a function of their ionic radius (Jambon, 1982; Wood and Blundy, 1997). The curvature radius of the parabola becomes higher with the valence of the cations, so that the largest cations are not necessarily the most incompatible

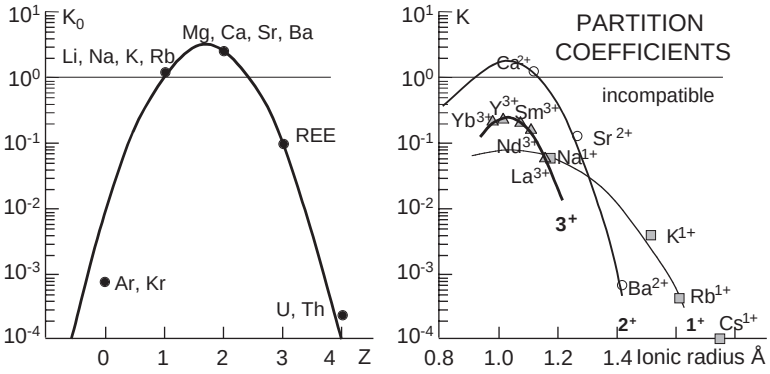

Fig. 4 Theoretical curves for partition coefficients values between melt and mineral. The curves are redrawn from Blundy and Wood (2003), who took clinopyroxene as an example. On the left in a) the theoretical value of the partition coefficient K_0 for a couple of elements with different valence. On the right, in b), the same curves, but now represented for partition into a clinopyroxene structure, emphasizing the valence of each group of elements. Those curves, with parabola shape have a maximum close to that of Ca^{2+} corresponding to the site of possible incorporation.

(Fig. 4). The maximum of the parabola corresponds to the optimum ionic radius of elements to enter a given crystallographic lattice.

The situation is much more complex when dealing with melts in which ions are ubiquitous. Ions, or even polymers, are more tolerant for incorporating an element with a different ionic radius. When dealing with both the ionic radius (r) and the charge (Z) of ionized elements, it seems easier to consider the ionic potential Z/r (Railsback, 2003). The ionic potential discriminates between hard and soft cations, and similarly for anions. The ionic potential of hard cations is the highest ($Z/r > 8$) and the cations present no outer-shell electrons. It allows distinguishing between anions, cations and metals, depending on their ionic charge (Fig. 5). Hence some elements can adopt different charges for combining with other elements. For instance, the occurrence of S in melts depends on the ambient conditions and on the valence state to which S is complexed. The various states of valence range from +6 in sulfate (e.g. $BaSO_4$), +4 in sulfite (SO_2), 0 (S), –1 (FeS_2) to sulfide with –2 (H_2S). It leads to numerous possibilities for S to form complex associations. This is quite important for ore forming minerals, since elements can combine differently from their ionic charge and their oxidation state. It allows discriminating elements in function of their ionic strength, separating anions from cations and neutral metals, but also between those elements with low strength, or LFSE as alkaline earths, from those with high strength (HFSE) as heavy charged metals as Sb, As, U, W, Mo, Cr, Te, Se and Re (Fig. 5).

Indeed, the summit of the parabola along which partition coefficients lie for elements with a similar valence (Fig. 4) is centered on the ionic radius and potential values for the considered mineral. In the diagram (Fig. 5) the

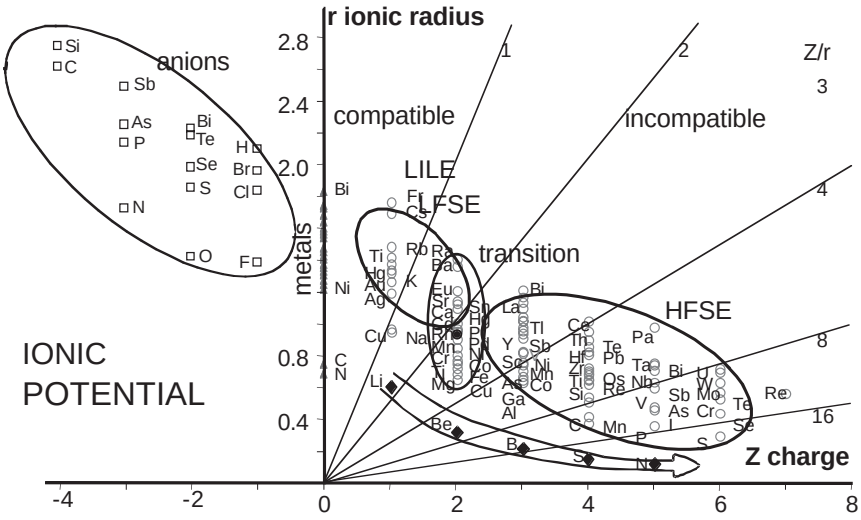

Fig. 5 Ionic radius versus ionic charge values for anions, neutral metals and cations, with possible different charge values. The diagram is drawn from Shannon (1976) and Railsback (2003) data, who provide values of ionic radius. It can be considered as a map, in which the parabola of the preceding figure (Fig. 4) would be a cross section for a given ionic charge. The main advantage of the figure is to emphasize the strength of heavily charged cations with small ionic radius.

black dot close to the valence for Ca^{2+} corresponds to the maximum compatible value for elements that would combine within a clinopyroxene, as shown on the values of partition coefficients adapted from Blundy and Wood (2003). This becomes even more complicated when the mineral presents several possibilities for accepting elements, as M1 or M2 sites in pyroxene. In the present case, only M2 site is the preferred of incorporation. The diagram can be used as a map to plot the most probable values of partition coefficients.

Nevertheless, in the case of melt, that incorporates a fluid phase, elements may enter different phases, since melt, crystal, fluid and gas may coexist. In consequence, a different partition coefficient should be used for $K^{melt/min}$, $K^{melt/fluid}$ and $K^{melt/vapor}$, which seriously complicates the computation of element behavior. The situation becomes complexes when examining the composition of the fluid phase, here referred as fluid and vapor. Hence the respective proportions in water and brines strongly differ in both cases. In addition the dissolved salts may enhance or lower metal solubility in the fluid phase.

Values for partition coefficients between melt and minerals $K^{melt/min}$ are extremely dependent on the magma composition (Rollinson, 1993; Bea, 1996) and on external variables (Blundy and Wood, 2003). Nevertheless, most published compilations of partition coefficients (e.g. Rollinson, 1993) are valid for basalts and basaltic andesites only (Roberts and Clemens, 1995). Data sets for granites are more difficult to establish (Sawka, 1988; Bea et al., 1994; Bea, 1996). Hence, the crystallized phases are usually in equilibrium with the co-existing glass composition in volcanic rocks. In consequence, the partition coefficients between mineral and glass are determined by measuring the element concentration in both components. In contrast, the composition of a granitic melt varies continuously while the mineral phases crystallize. The mineral assemblage observed at the end of the crystallization represents the only record of the crystallization history. Therefore, one must first estimate the starting magma composition as well as the succession of mineral phases during crystallization. Such estimates induce bias in estimating the partition coefficient while felsic magmas evolve (Bea, 1996). The composition of melt inclusions also provides indication on the evolving state of the magma. They allow more precise determinations of partition coefficients, and studies using LA-ICP-MS on fluid and melt inclusions are in progress (Webster et al., 1997; Thomas and Klemm, 1997; Chabiron et al., 2001; Halter et al., 2002; Rusk et al., 2004).

The second difficulty inherent to felsic magmas is the presence of accessory minerals in which a lot of inclusions present high concentrations in trace elements. This contradicts the principles of equilibrium crystallization that rules the determination of partition coefficients. For example, biotite and alkali-feldspar are good host-minerals for allanite, monazite, zircon, apatite and xenotime, which are in turn potential hosts for all rare earth elements (Bingen et al., 1996). Consequently, the determination and use of a set of partition coefficient for felsic melts often remains of uncertain use. Values of partition coefficients between melt and the vapor phase are still very scarce and only exist in very specific conditions for Mo and Sn (Williams-Jones et al., 2002; Migdisov and Williams-Jones, 2005; Rempel et al., 2006). In addition the chemical content of the fluid phase has a direct control on the partitioning (Frank et al., 2003).

Partition coefficients indicate how elements distribute themselves between the considered phases so that at equilibrium, all chemical potentials, or Gibbs free energy, in each phase should be equal according to Henry's law. Each of them is the sum of the initial chemical potential plus a function of the activity coefficient. The ratio of elements is the ratio of the Henry's constant for each phase and an exponential function of the initial difference of the free Gibbs energy (ΔG) normalized by temperature

through the perfect gas constant. Therefore the values of enthalpy (ΔH) and of entropy (ΔS) of melting control the value of partition coefficients with temperature, provided there is neither volume nor pressure change (Blundy and Wood, 2003). The last condition may be considered as second order, thus provided the values of enthalpy and entropy of melting are known, the partition coefficients can be computed.

$$K^{min/melt} = \exp(-\Delta G/RT) \quad (13)$$

This requires a lot of thermodynamic data, which at present are not available for all elements, all minerals and sites within those minerals. Nevertheless, synthetic values can be computed, assuming a bulk value for enthalpy and entropy of melting. They provide indication on how partitioning operates as a function of temperature. In addition, it should be pointed out that the exact values of $K^{min/melt}$, are necessary for computing fractionation, but they are not when examining the evolution of the melt. In contrast, estimating its variation when a felsic melt suddenly increases in temperature from 600 to 900°C because of an intrusive mafic magma suddenly cooled from 1200 to 900°C is important. In that case, the partition coefficients in the felsic melt vary from 110 to 5, inducing a flux of elements from the mafic to the felsic magma. However, it should be noted that a present, the exact computation of $K^{min/melt}$ through thermodynamic data for a given pair of mineral and element cannot be realized because those data often lack. Nevertheless, calorimetric data exist for silicates melts (Navrotsky, 1990; Kojitani and Akaogi, 1997) that allow estimating and bracketing the required values of melting enthalpy and entropy.

Values for melting enthalpy are in the range 25-75 kJ/mole for most silicate melts (Richet and Bottinga, 1984, 1986; Richet and Fiquet, 1991) or organic compounds (Gilbert, 1999; Chickos and Acree, 2003) at low pressure (< 0.5 GPa). Close to melting temperature, a little higher than 1000°C, the enthalpy and entropy are roughly in the ratio of 1000. The values of entropy (ΔS) are bracketed between 25 and 75 J/K/mole (Iwamori et al., 1995; Hirschmann et al., 2003). In consequence, theoretical values of partition coefficients are computed from Equation 13 for enthalpy ranging 25 to 75 kJ/mole and entropy ranging 30-60 J/K/mole to estimate the variation of $K^{min/melt}$ in the interval 600-1200°C (Fig. 6).

The variations with pressure can be neglected since magma intrusion occurs at depth levels that can be considered as constant. The partition coefficients decrease with temperature (Fig. 6). The decrease is about 1 order of magnitude for a temperature shift of +300°C. The higher the enthalpy of melting, the higher the K value for a given temperature. The variation is about 1 order of magnitude when the enthalpy is increased by 20 kJ/mole, between 25 to 75 kJ/mole. The value of K is also shifted by about 1

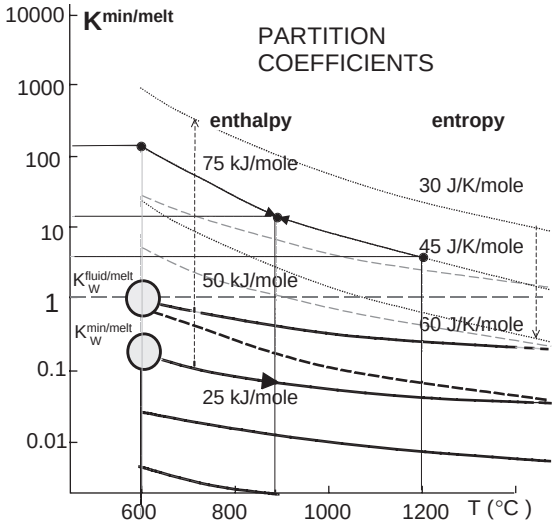

Fig. 6 Theoretical values of partition coefficients as a function of their melting entropy, from 30 to 60 J/K/mole, with increasing values downward. Those are plotted for respective values of melting enthalpy, for 25, 50 and 75 kJ/mole, and respectively represented by points, dashes and fine lines, with increasing values upward. The place for W-bearing melt and fluid are indicated by grey circles, with the trend of variation of partition coefficients between melt and the fluid and mineral phase.

order of magnitude when the value of entropy (ΔS) is decreased by step of 15 J/K/mole between 60 and 30 J/K/mole.

When considering Sn and W, the partition coefficient for W between crystal and melt is commonly lower than unity, with value close to 0.05 (Candela and Bouton, 1990). It makes W incompatible in the solid phase, and its concentration increases in a reducing melt. In contrast the fluid/melt partition coefficient for W is close to unity, resulting in a concentration of W in the fluid phase before reaching water saturation (Candela and Holland, 1986; Candela, 1992). When a new intrusion of magma occurs, whatever its chemistry, the partition coefficient is depressed a little more, resulting in more incompatibility in the solid phase with respect to the melt. In contrast, the fluid phase is augmented in value, which increases its partial pressure, thus increasing the value of the partition coefficient. In consequence, new magma intrusions, provided they are hotter than the magma chamber, and it is generally the case, contribute to segregate W within the fluid phase. Solubility of Sn is very dependent on the alkaline character of the magma (Fig. 7) (Linnen et al., 1996; Linnen, 2005). Nevertheless, for peraluminous or crustal-derived magma, the solubility is of the order of 0.05 resulting in poor compatibility. From recent experimental studies on Sn solubility directly in the vapor phase, the values of log $K^{gas/liq}$ varies from –10 to –4, depending on the oxygen fugacity and decreasing pH, resulting from Cl ions present in the liquid phase

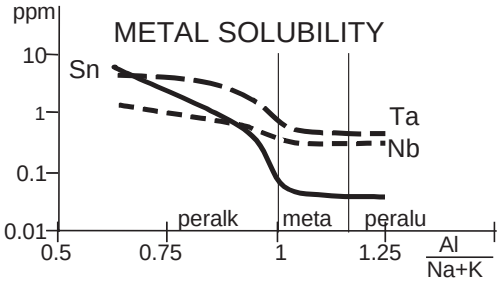

Fig. 7 Metal solubility in felsic magmas for Sn and associated Ta and Nb as a function of the alkaline character of the magma. Data are taken from Linnen (1998) and related papers.

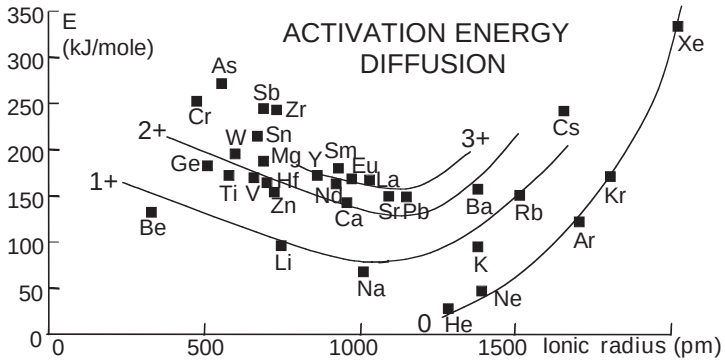

Fig. 8 Plot of activation energy for elements in function of their ionic radius. Elements are grouped by ionic charge, denoting a parabolic correlation between them.

(Migdisov and Williams Jones, 2005). It results that the volumes of Sn that can be transported in Cl-bearing water gas are greater by several orders of magnitude compared to those carried in a water-free system.

5. Diffusion Variations with Temperature

Diffusivity depends exponentially on temperature (T) through an activation energy (E, H, or Q), linked to temperature by the perfect gas constant (R). The relation writes

$$D = D_0 \exp(-E/RT) \qquad (14)$$

The value of the activation energy depends on the ionic radius, the electronic charge of the considered element and the Young's modulus of the site. Hence, the activation energy estimates the ability of the element to diffuse in a sphere (Frenkel, 1946; Anderson and Stuart, 1954). The relation was later modified (Brice, 1975) by considering the strain required to expand the network. The relation takes a parabolic form as a function of the ionic radius of the elements, with curvature inverse to that of partition coefficients (Figs. 4 and 8). It goes through a minimum, corresponding to the optimum radius of strain-free substitution.

From about 40 values of activation energy in felsic melts found in the literature (Hoffmann, 1980; Jambon, 1982; Mungall et al., 1999; Koepke and Behrens, 2001), the values range from 33 for He to 348 kJ/mole for Xe; but data for heavy and charged elements as P lack. Nevertheless, comparison is not always possible between data sets because values were not measured in similar pressure conditions. The emerging feature from this compilation is that most values of activation energy, provided gas and volatile elements (noble gas, Be, Li) are not considered, range between 120 and 280 kJ/mole, with an average around 185 kJ/mole.

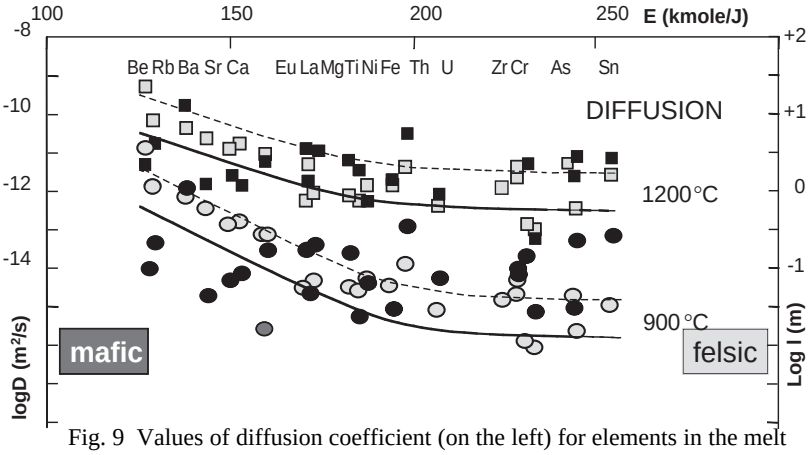

Fig. 9 Values of diffusion coefficient (on the left) for elements in the melt as a function of their activation energy with the corresponding characteristic lengths on the right. Some important elements are indicated for reference, however, note that not all elements are pointed. Two sets of data are considered, depending on whether the melt is mafic (in dark grey) or felsic (in light grey). Trends are indicated displaying diffusion values for temperatures of 900 (circles) and 1200°C (squares), showing that activation energy controls diffusion with temperature.

Element diffusion in the melt is computed for temperature of 900 and 1200°C (Fig. 9), and this for values measured in granitoids (Mungall et al., 1999) and basaltic melts (Hoffman, 1980). The logarithmic value of diffusion coefficients can be considered as linear against the low activation energy when plotted for a given temperature. However, the slope changes for two different temperatures. For high activation energy (> 200 kJ/mole), diffusion remains constant. Departures to the linear trend are attributed to errors in the determination of the diffusion coefficient or in the activation energy. Hence, experimental values were measured, in various conditions of temperature and with different melt compositions. The difference between mafic and felsic melts has been studied from isotopes self-diffusion (Lesher, 1994). Nevertheless, diffusivity in mafic magma is commonly one order of magnitude larger than in felsic melts. Plotting diffusion values

measured in basalt and in granite has not been more useful (Fig. 9). Indeed, it remains difficult to compare existing experimental values in spite of a large compilation of papers.

The trends displayed by the two curves at 800 and 1200°C for one type of melt have two interesting aspects (Fig. 9). First, they present a different slope and the difference between them increases with the largest values of activation energy, hence the larger or heaviest elements. Second, they show a nearly linear trend for low activation energy, allowing an approximation that will disregard the errors introduced by the measurements, and those relative to the chemical composition of the melt. Such correlations have already been noted (Winchell, 1969; Hoffmann, 1980). Hence, the trends indicate that the melt composition is of second order compared to the trend introduced by the values of the activation energy. Therefore, it is possible to reason only on the values of the activation energy, ignoring in a first step which element (compatible, incompatible) and which magma (i.e. with different composition) are considered for diffusion.

A model is thus constructed, that considers the temperature of intrusion of a new magma into a former one. The two magmas rapidly reach an equilibrium temperature in their contact zone. The time scale is defined from the time interval that separates two intrusions (Petford et al., 2000). The characteristic length of diffusion (Eq. 6), computed from the diffusivity with temperature (Eq. 14), determines the re-distribution of elements (Fig. 9).

It was not possible to compute the variation in the values of partition coefficients because it basically depends on which mineral phase is concerned. In consequence only theoretical curves, calibrated in entropy and enthalpy values were designed as a function of temperature. A sudden change in temperature alters the value of partition coefficients by modifying their magnitude. When the partition coefficient becomes less than one, the element suddenly becomes incompatible. However, the real effect is not to consider compatible and incompatible elements, but to estimate the order of magnitude a compatible (or incompatible) element can be.

6. Magma Intrusions and Diffusion Variations

In a first order examination, two cases of intrusion are considered for mafic and felsic magmas interactions (Fig. 10). The yet emplaced magma at depth, about 500 MPa, corresponding to a deep crustal intrusion, is taken as felsic. It could represent a granitic magma chamber, essentially peraluminous, in order to develop Sn-W ore deposits. Crystallization has already started and the temperature is 200°C below the liquidus, namely 600°C for the felsic magma. It corresponds to about 33 % of crystal formed. The initial water content is fixed at 10 %, with

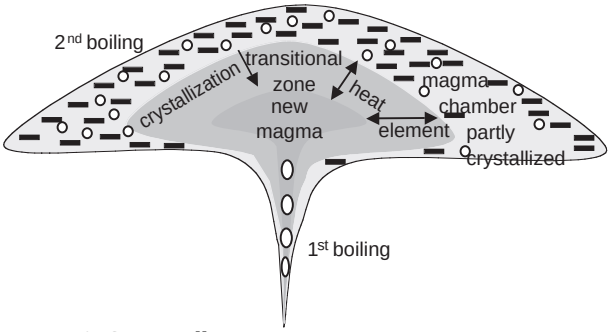

Fig. 10 Cartoon illustrating magma intrusion into a previous magma chamber. The magma chamber bears first formed crystals and the fluid phase corresponding to second boiling. In contrast, the new intruding magma is crystal-free, but also includes a fluid phase corresponding to magma decompression (first boiling). In the transition zone, the temperature contrast between the two magmas redistributes the elements.

CO_2 content at about 0.6 % and a total amount of S of 1000 ppm. After partial crystallization, those initial values are lowered by one third in the melt. About 3.33 % of the fluid phase have already been exsolved and remains in the melt as bubbles. Its bulk composition is then 94.3 % of water, 5.6 % of CO_2 and 1% of S. The viscosity of this magma, which was originally at 106 Pa.s, is now at 109.1 Pa.s after cooling and crystallization (Eq. 1). The new incoming magma is hotter and free of crystals, but with a possible small restitic content. It has respectively 800 and 1200°C in case of felsic or mafic intrusion. The intrusion is not time dependent. The temperature at the contact is the average between the two magmas (Fig. 10). The time interval between intrusions is fixed at 30 ky.

The first case examines a felsic intrusion into a magma chamber of similar composition, but with a lower temperature. In a second set, a cold felsic magma is intruded by a hotter mafic one. In each case, the changes in the characteristic length are computed for the former magma and the new intrusion. The characteristic length decreases in the new magma, since it cools and the length increases in the initial magma, warmed by the new intrusion (Figs. 11 and 12).

6.1. Felsic intrusion into a felsic magma

It corresponds to the common case of building up a granitic pluton, as observed in many continental collision zones. The new felsic magma has a temperature of 800°C and it is free of crystal. It has the characteristics of the initial magma that formed the magma chamber. The temperature interval between the two magmas is of 200°C. At the contact, the temperature rapidly drops and increases by ± 100°C resulting in a transition zone. Its width is approximated from the characteristic length computed from thermal diffusivity, providing a value of 1 km reached trough the adopted time scale of 30 ky.

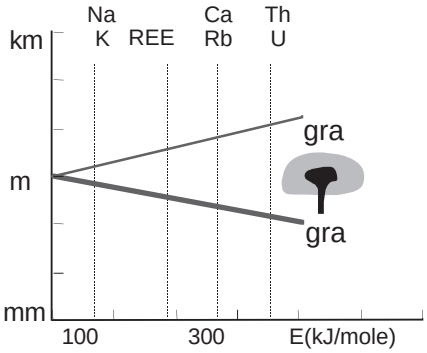

Fig. 11 Change in the characteristic length of diffusion as a function of the activation energy. The case represents a felsic hot magma (800°C) intruding a colder (600°C) felsic magma chamber (in grey). The difference in temperature is small and the each magma respectively cools and warms. The associated variation in diffusion length increases (in grey for the magma chamber) or decreases (in black for the new magma) by a maximum of 1 order of magnitude. Values of activation energy for alkaline, rare earth and some metals are indicated.

The temperature and viscosity contrast between the two magmas may induce thermally driven convection. Its scale may be estimated to be less than some mm.

The change in temperature has effects on the characteristic lengths associated with diffusion and on partition coefficients. The activation energy controls the diffusion length. Taking a variation of ± 100°C around 700°C, the order of magnitude of the diffusivity values are changed by a factor of 0.75 for the smaller activation energy, but by a factor of 1.6 for the larger activation energy values. For a period of 30 ky, the variation in diffusion length also varies from 0.75 to 1.6 (Fig. 11). It results that depending on the considered element, diffusion of alkaline elements (Na, K) is practically unchanged, whereas REE can move about 50 cm further. In contrast for the elements with high activation energy (Sn, Sb, Zr) the distance of diffusion increases for more than 1.6 orders of magnitude in scale (Fig. 11). However, owing to the composition of both magmas, the change in composition of the intermediate zone is quite insignificant. Hence, most of the major elements (Si, Na, K, Ca) have low activation energy and are not easily activated by a change in temperature.

The change in the values of partition coefficients is about 1 order of magnitude, decreasing in the new magma, and increasing in the former one (Fig. 5). Considering an elevated value of enthalpy corresponding to highly incompatible elements, some initial values of $K^{min/melt}$ of 500 could drop to 50 in the former magma, whereas the value for the same element could increase from 5 to 50 in the new magma. Experiments indicate document that partition coefficients between REE and lherzolite melts increase from 0.2 to 2 when temperature increases from 1000 to 1500°C (McDade et al., 2003). In contrast, the variation is more restricted for Mn and Zn (Kohn and Schofield, 1994), certainly owing to a lower melting enthalpy. A switch from incompatible to compatible element may take place for those elements presenting a low melting enthalpy and moderate melting entropy or for those with high melting enthalpy and high melting entropy (Fig. 5). In the case of W and Sn ore formation (Fig. 5), the value of $K^{min/melt}$ for W is about 0.5 (Candela, 1992), and is lower than 1 for $K^{fluid/melt}$ (Keppler and Wyllie, 1991) whereas the values for Sn seem quite lower (Linnen, 1998).

The amount of the fluid phase is surprisingly few affected by the intrusion of a new magma. Hence the increase in temperature of the former magma in the boundary zone is compensated by the decrease in temperature of the new one. Hence the quantity of fluid exsolved by the sudden crystallization is equal to the quantity of fluid that can be dissolved in the warming magma. This is valid provided the two magmas have a similar composition and amount of saturation pressure of gas.

6.2. Intrusion of a mafic hot magma into a colder felsic one

A new batch of mafic magma at 1200°C is introduced while the earlier, felsic is yet partly crystallized with a temperature of 600°C. The new magma has a viscosity of 100 Pa.s. Its fluid phase content is fixed at 3 % of water, with 0.2 % of CO_2 and 5000 ppm of S, therefore with internal proportions of 81.1, 5.4 and 13.5 % respectively. The temperature difference is huge. At the contact between the two batches, the temperature soon reaches 900°C (Crank, 1975), inducing a variation in temperature of ± 300°C in both magma batches. Cooling by 300°C results in a having about 50 % crystals formed in the mafic melt, thus half of its fluid phase exsolved. The time and length constants for crystallization overlap with those for diffusion (Fig. 3). It makes possible the re-incorporation into the warming melt of the fluid phase exsolved from the cooling melt.

The initial magma is partly crystallized at 600°C with viscosity of $10^{9.1}$ Pa.s. The intrusion suddenly warms it to 900°C, thus it becomes free of crystals and with viscosity $10^{4.8}$ Pa.s using an Arrhenian viscosity with activation energy of 300 kJ/mole (Maaløe, 1985). It becomes thus more fluid than the initial magma that entered the magma chamber at 800°C. In contrast, the viscosity in the mafic magma increases to $10^{3.7}$ Pa.s due to cooling, and to $10^{4.7}$ Pa.s when taking into account the crystal content (Eq. 1). The fluid phase is also strongly modified when considering the saturation curves (Fig. 2). Because the mafic magma cools down and crystallizes, its water and CO_2 contents are halved and decreased to 1.5 and 0.1 % respectively. Those fluids can easily be re-incorporated into the felsic magma from which a large part of its fluid content has already been exsolved, but that is suddenly

brought to 900°C. Conversely, S is partly exsolved from the mafic magma, but cannot be re-incorporated into the felsic melt, which still has 666 ppm of saturated S (Fig. 2). The remaining S, about 2500 ppm should be added to the 333 ppm already in the fluid phase. This modifies the relative proportions within the gaseous phase, which is now formed by 72.2 % H_2O, 7.3 % CO_2 and 20.5 % S. It increases the proportion of S and CO_2 relative to water in the fluid phase. It seems that halogen fluids adopt the same behavior as S, increasing and modifying the chemistry of the fluid phase. The above reasoning does not take into account the possible changes in redox conditions that may be induced by the intrusion of a mafic magma (Clemente et al., 2004), nor it takes into account solubility variations with temperature.

This intrusion scheme also drives the magma toward totally different conditions from a steady-state cooling of the magma chamber. The former felsic magma suddenly becomes over-heated, whereas the mafic magma is strongly cooled. This contrast in temperature and viscosity may induce thermally driven convection, but with a scale of about 24 cm.

The large variation in temperature, ± 300°C, deeply alters element diffusion in both types of melt. The characteristic lengths may vary by two orders of magnitude (Eqs. 6 and 13) for elements with high activation energy (Fig. 12). The large temperature variation means a larger exponential value for any activation energy, thus a larger change in the characteristic lengths. The change is not symmetric, being more important in the cold felsic magma because temperature enhances diffusion. The characteristic lengths increase by two orders of magnitude for an activation energy of 250 kJ/mole in the felsic magma. Comparatively, the change is only 1.2 orders of magnitude for the same activation energy in the mafic magma (Fig. 12). The variation in the partition coefficients induced by the ± 300°C is ± 1 order of magnitude in the felsic and mafic magma respectively for elements with high melting enthalpy, but only ± 0.5 order of magnitude for those with high melting enthalpy (Fig. 6). In that case, the dependence of partition coefficients on melt composition may result in larger effects. Experiments indicate document that partition coefficients between REE and lherzolite melts increase from 0.2 to 2 when temperature increases from 1000 to 1500°C (McDade et al., 2003). In contrast, the variation is more restricted for Mn and Zn (Kohn and Schofield, 1994), certainly owing to a lower melting enthalpy. In the case of Sn and W, the values of the partition coefficients become less, making those elements more incompatible in the solid phase. They are driven to the fluid because the value of $K^{min/melt}$ for W is below 1 (Candela, 1992) whereas the value for $K^{fluid/melt}$ is even lower, especially if brines are present in the fluid phase (Kepler and Wyllie, 1991). The values of $K^{fluid/melt}$ for Sn are two orders of magnitude lower than 1 in brines (Keppler and Wyliie, 1991; Linnen, 1998; Linnen et al., 1996).

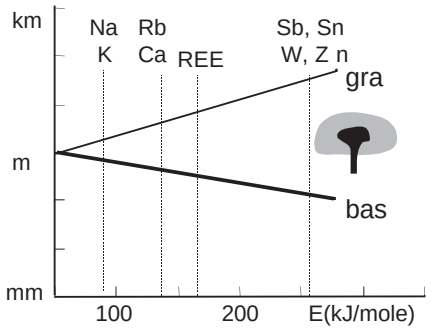

Fig. 12 Same as Figure 11 but for a mafic and hot (1200°C) magma intruding a felsic magma chamber partly crystallized at 600°C. The symbols are similar to those on Figure 11. The effect is exacerbated due to the large temperature contrast between the two types of magma. The change in the characteristic length may reach two orders of magnitude. The effect is reinforced in the felsic magma, while it is damped in the mafic one. Therefore elements concentrate from the mafic toward the felsic magma.

7. Discussion

7.1. Limits and significance of the results

This approach to element diffusion during successive magma inputs is by evidence oversimplified. It has been conducted as a first-order test to demonstrate the ability of elements to recombine while a granitic body is built. Assuming that about 30 ky separate two magma intrusions provides a time scale during which diffusive processes can take place. By evidence, this is too short for diffusion to affect already solidified minerals (Fig. 3). In contrast, it gives time for heat to diffuse, i.e. to enough cool down so that the magma may reach rigidity. This takes place for intrusions of which the size is small enough, less than one kilometer. Considering those limits in time and scale, magma motion and element diffusion are activated, that can lead to element redistribution.

In case of successive magma inputs, elements diffusion is obviously limited to the melt. The effect on solids is negligible in a first approach. This is the case for instance in xenoliths and enclaves. The amplitude of diffusion is enhanced for the intrusion of a mafic magma into a felsic one. In case of a felsic intrusion into a mafic one, the redistribution is restricted to a boundary layer at the interface between the two magmas. The diffusive effects on viscosity and element distribution are restricted to a metric scale (Fig. 3) in case of magma intrusion into a magma chamber of similar composition.

The diffusive effects operate in both magmas, the former and the new one, though they are contrasted. Hence,

the former magma is heated by the new intrusion, which enhances diffusion effects. In contrast, the new magma is rapidly cooled at the contact with a former magma, slowing down diffusion. This is specifically true for mafic magmas which are always cooled, thus reducing the diffusion within them. In contrast, the diffusion effects are amplified by heating in felsic magmas.

The diffusive effects are function of the temperature contrast between the former and the new magma and the amplitude of the effect is function of the activation energy for each element. However, the effects are contrasted when considering diagrams plotted in function of the activation energy (Figs. 11 and 12). When plotting the values of the diffusion coefficients at different temperatures, the values decrease with the activation energy (Fig. 9). In contrast, when submitted to a sudden temperature increase, the effect is positive with the activation energy. The more important the activation energy, the more mobile is the element when temperature increases. This effect largely compensates the decreasing value of the diffusion coefficient.

7.2 . Volume fraction of the new input

In the model, the intrusion of a new magma is instantaneous, as well as the change in temperature it induces in the magma chamber. This is an over-simplification that can be justified to examine the consequences of the intrusion. In reality the change in temperature is progressive and should take into account the volume fraction of each magma batch (ϕ) to determine the final temperature of equilibrium. Therefore, the respective heat capacity (C_m, C_f) and density (ρ_m, ρ_f) for each magma batch should be taken into account, assuming m and f indices for the mafic and felsic magma.

$$T = (T_m - T_f)\, \phi\, \rho_f\, C_f / (\phi\, \rho_m\, C_m + \rho_f\, C_f) \qquad (15)$$

In the present case, the initial temperature of the felsic and mafic magmas are selected at 800 and 1200°C. The heat capacity values are 1200 J/K/kg for the mafic and 1000 J/K/kg for the felsic magma. The density of the melts is 2700 and 2300 kg/m^3 respectively. A curve can be computed that indicates the final temperature of a mafic injection of relative volume f. The computed temperature rapidly reaches the asymptotic value corresponding to the temperature average between the two magmas (Fig. 13). In case of very small volume fraction, the equilibrium temperature is lower than the temperature difference. For instance it is only 200°C for a contact mafic-felsic initially with 400°C difference, if the volume of the mafic magma is 1.41 of the total volume. The variation in temperature is naturally in the cooling magma (Fig. 13). This situation should be valid for enclaves, which do no present enough massive heat to reach equilibrium. In all other situations, the conditions of diffusion should be satisfied.

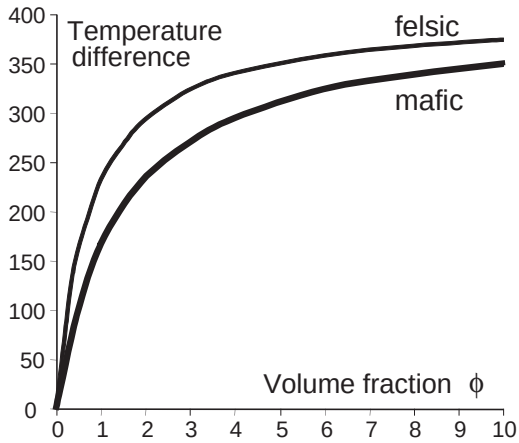

Fig. 13 Temperature variation according to the heat capacity of the mafic (in black) and felsic (in grey) magmas, when the respective volume percentage of new magma is small compared to the magma chamber. The initial temperature difference between the two magmas is 400°C. It corresponds to the asymptotic value of equilibrium.

7.3. Diffusion or convection

A much faster redistribution of elements should operate if mixing is accelerated by magma motion, i.e. through convection. There has been a considerable debate about convection in magma chambers and plutons (Brandeis and Jaupart, 1986; Marsh, 1989; Flinders and Clemens, 1996; Bergantz, 2000). However, those studies examined generally a huge magma chamber, built from a single input of magma, and commonly considered as a closed system.

Interactions between particles and melt, including a gaseous phase, have been examined by independent scaling (Burgisser et al., 2005). They provide a framework to scale magmatic systems since they do not have to take into account the complex feedback reactions between the phases (Burg and Vigneresse, 2002). The three non-dimensional numbers examined are the Reynolds (R_e), Stokes (S_t) and a Stability number (Σ_t). The first one indicates the regime of the melt flow, and its limits of stability. The two others describe the dynamic behavior of the particles within the magma (Burgisser et al., 2005). Low Reynolds numbers characterize laminar flow in which the shear flow imprints a fabric to first formed crystals, as presently observed in most granitic bodies (Bouchez, 1997). A positive stability number characterizes dynamic motion of the particles, by buoyancy for instance. However gradational layering is often observed (Clarke and Clarke, 1998) and accumulation of heavy mafic enclaves in the upper part of a felsic magma chamber has been described (Wada et al., 2004). A positive Stokes number characterizes a regular settling of the particles. Evidence of local diapir-like features (Weinberg, 1999),

intrusion-like fountains (Collins et al., 2000) or turbulent flow structures (Wiebe and Collins, 1998) are observed in many granitic bodies. Their scale is generally below a metric scale. This leads to suppose that the boundary layer associated to magma inputs is commonly restricted to a metric scale (Snyder, 2000).

7.4. Open or closed system

Should a magma chamber be considered as an open or a closed system is a recurrent problem. Many models of chemical evolution of a magma chamber identified the pros and contras of both systems (review in Spera and Bohrson, 2001 references therein).

Theoretical models of the interactions between dynamics and the thermo-chemical evolution of a magma chamber have been considered (Mourtada-Bonnefoi et al., 1999; Snyder et al., 2004). Actually, the rheology of a magma chamber and its chemical composition make it fundamentally like a non-adiabatic open system. This profoundly differs from a basaltic magma that can be traced through adiabatic decompression melting. A granite pluton behaves as an open system by the successive inputs of primitive melts that may be felsic or mafic, as attested by the ubiquitous observations of dikes of various composition (Collins et al., 2000). However, a magma chamber evolves rapidly toward a steady state owing to the short timescale of all processes (Mourtada-Bonnefoi et al., 1999).

Because of the continual mixing of magmas, in various proportions, the question could be addressed to consider all granitic magmas as hybrid magmas. Certainly, this assumption may be provocative, and not compared to the usual definition of hybrid granitic magmas, or H-type magmas (Castro et al., 1991). The point merits to be questioned, since it is a direct consequence of mingling felsic and mafic magmas (Weinberg and Leitch, 1998).

Fluids circulation in the surroundings of the intrusion should also be considered as part of some open system. Because the intrusion creates a thermal anomaly, it induces water flow in the permeable country rocks (Cathles, 1977). However, there is some delay between the time of the intrusion and that of initiation of thermally induced fluid convection. The conditions for the intrusion indicate it took place at 500 MPa (Fig. 1), equivalent to about 17 km at depth for the floor, and with a roof at about 12 km in depth. An estimate of the time for water convection to start may be approximated by the diffusion time for heat to reach about 2 km below the surface, the basement under the sedimentary cover. The resulting 10 km gives the order of time (3 My from Eq. 6, for simplicity) before water convection starts. This matches the time delay observed in many deep intrusion showing thermo-magmatic Sn and W ore deposits (Chen et al., 1993; Pettke et al., 2005). Once established, the magmatic effects progressively give place to pure hydrothermal circulation (Heinrich et al., 2004). The hydrothermal circulation can last for several tens of My (Cathles et al., 1997).

7.5. Signification of the time delay

One important assumption of the present model is the time lag existing between magma intrusions. It has been fixed at 30 ky, on basis of observations averaging the construction of granitic bodies (Petford et al., 2000) and magma segregation (Rabinowicz and Vigneresse, 2004). If intrusions develop on a slower basis, elements have more time to diffuse, thus developing over a longer length. However, because heat diffusion is much faster than element diffusion, a too slow sequence of magma inputs may result in having the former magma already crystallized, and thus unable to exchange elements. Two situations may develop. In the first case, the yet emplaced magma reached full crystallization. This may take between 50 and 100 ky for an intrusion 2 to 3 km in size if adopting an average rate for crystallization within a cold crust ranges about 50 to 200 mm/yr (Vigneresse and Améglio, 1999). Therefore doubling the time for magma intrusion would not let diffusion to spread. In contrast, if magma is delivered with a faster rate, then time is not left for elements to diffuse. In this case, again, diffusion can be damped, though too rapid intrusions would not let time for the emplaced magma chamber to cool, and thus decreasing the temperature contrast between magma intrusions. Thus progressively, repeated intrusions could keep warming the whole magma chamber, delaying time of crystallization. The residual liquid could thus find time to diffuse at larger distances.

8. Implications for Sn-W Ore Formation

The paper started by examining the implications successive magma inputs, with different composition and temperature, could bear on the genesis and formation of Sn-W ore deposits. Obviously, the thermal perturbations associated with new and hotter magma contribute to segregate metals, by decreasing their solubility in the melt. Thus metals are confined with the fluid phase. However, enhancing element diffusion and partitioning is not enough to lead economic concentrations of metals. Then, it can be interesting to examine the other processes that yield to ore formation. Among them, the internal crystallographic structure of those minerals that bear ore seems important, as already noted for the implications on diffusion and partitioning. Those elements with M^{4+} ions imply a high ionic potential (Fig. 5), which has influence in forming complexes with halogen anions.

8.1. Crystallographic aspects and associated elements

The magmatic conditions examined in the present

paper are essentially related to felsic magma, reduced and crustal-derived. In those conditions Sn and W are the major associated elements giving place to economic ore deposits. According to the redox conditions, those minerals are often found with an oxidation state of 4 and coordination number of 6, as cassiterite (SnO_2), pyrolusite (MnO_2) or rutile (TiO_2). Crystals from the rutile group pertain to the tetragonal system with the oxide ions in a hexagonal close-packed arrangement (Burdett, 1995). The insertion of the metal with valence +4 into the octahedral holes causes the structure to expand in order to prevent contact between the metal and the oxide ions (Eyert et al., 2000). Adopting a hcp (hexagonal close packed) structure results in having two oxide ions in the hcp unit cell, in a ratio 0.5, according to the similar ratio of the metal relative to oxygen atoms.

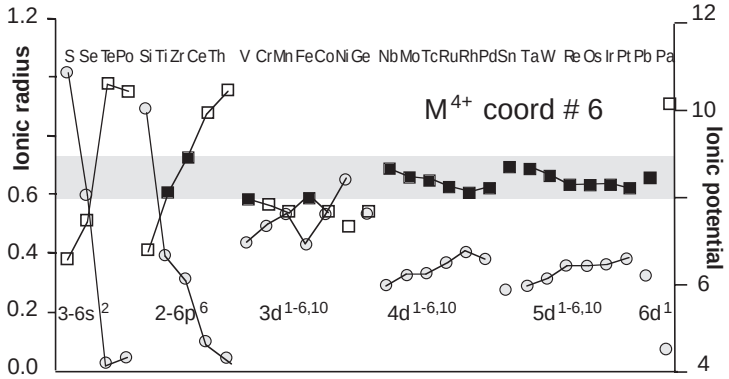

Fig. 14 Ionic radius (square) and ionic potential (circle) represented for all elements having a M^{4+} valence and coordination number of 6. Elements with 6d and 5f electronic structures are not represented, because of their too large ionic potential. From all those elements, those which present an ionic radius similar to Ti can enter the rutile group structure (black squares).

Going back to ionic radius considerations (Figs. 5 and 8), it appears that other elements present similar ionic potentials with similar oxidation state and coordination number. The reference value for the ionic potential of Ti^{4+} is 6.61 and 0.605 Å for its ionic radius (Shannon, 1976). All ions having a slightly smaller ionic radius and same ionic conditions will present affinities with the rutile group. Looking to tables of ionic potential (Shannon and Prewitt, 1970; Shannon, 1976) allows selecting those elements (Fig. 14). Those elements, which have the required valence and coordination number, present four different electronic configurations. First, a group presents a $3\text{-}6s^2$ configuration, but none has its ionic potential close to 6 (Fig. 14). A second group presents configuration $2\text{-}6p^6$ and includes Ti^{4+}, the reference value. In this group, only Zr^{4+} presents a similar ionic potential and slightly larger ionic radius. The three other groups are more interesting since they include suites with 3d, 4d and 5d structures. The first of those groups with $3d^{1\text{-}6}$, and $3d^{10}$ structure includes V, Cr, Mn, Fe, Co, Ni and Ge. The ionic potential increases slightly with the filling of the d electronic layer, and it always remains higher than 6.84. It means that it can be difficult for those elements to substitute within the rutile structure. Only V^{4+} and Fe^{4+} could integrate that structure. The second group considers filling the 4d, from $4d^{1\text{-}6}$, and $4d^{10}$ structures. It includes Nb, Mo, Tc, Ru, Rh, Pd and Sn (Fig. 14). The value of the ionic potential increases with electronic filling, and the ionic radius decreases accordingly from 0.68 to 0.60 Å, allowing an easy substitution in the rutile structure. The last group, related to the layer 5d, from $5d^{1\text{-}6}$ and $5d^{10}$ structures, presents similar characteristics and includes Ta, W, Re, Os, Ir, Pt and Pb (Fig. 14). Elements that fill the structure 6d have not been considered here, since their ionic radius is large and commonly around 1 Å (Fig. 14).

The similarity of the electronic structures allows easy substitution and similar chemical affinities between those metals, provided their ionic radius is similar or smaller than that of Ti^{4+} (Fig. 14). Hence, Ti and Zr are often found together, both associated with felsic magmas when they occur within a magmatic context. They form mineralized cap rocks over anorthosite bodies and occur as oxides such as nelsonite (Kolker, 1982) or are associated to other rare metals in alkaline magmas (Kovalenko et al., 1995). Sn and W are commonly associated in ore deposits (Dietrich et al., 2000; Cerny et al., 2004) as well as they occur often with Ta and Nd and the columbo-tantalite suite in late magmas (Cuney et al., 1992) and pegmatites (Cerny et al., 2005). Mo, Re and Tc are known to share a same behavior (Hannah and Stein, 2002). Ru, Rh, Pd, Os and Ir exhibit similar properties as Pt and they are referred to as the platinum group elements (PGE). The large variety of occurrence or finding those elements in such different geological and magmatic context points to some other effect that would operate during metal segregation.

Sn-W mineralization with minor occurrence of La-Nb, associated with lighter elements as F, Li and Be is quite common in the Variscan domain of Europe (Tischendorf, 1988, Cuney et al., 1992; Raimbault et al., 1995), as well as with the very late peraluminous granites associated with the rapakivi granites (Haapala, 1997). Those elements are associated with the latest magmas, highly peraluminous. They are commonly interpreted as the result of magma interaction, with an important fluid phase demonstrated by the presence of F- and Li-halos developed in the surrounding rocks (Cuney et al., 1992).

The development of a fluid phase is also the place during which oxygen fugacity increases. Sn solubility varies by about two orders of magnitude (Fig. 7) depending on whether a magma is peralkaline or peraluminous (Linnen, 1998, 2005). A similar variation (Fig. 7), but with less

amplitude, is observed for La and Nb solubility (Linnen and Kepler, 1997).

8.2. Effects of magma replenishment

The combination of both factors, the value of the activation energy and the nature of the magma, i.e. its cooling or warming, makes the more energetic elements, i.e. the heaviest and the most charged with large ionic radius, preferentially mobile within felsic magmas. In contrast, their mobility is reduced within cooled down mafic magmas. Since the diffusive effects are more pronounced when a mafic magma intrudes a felsic one, the more mobile elements are sucked from the mafic toward the felsic magma. Elements, as As, Sb, Sn or W amongst base metals, present high activation energy. They are very mobile during magmas interactions.

The consequence of repeated magma intrusion on the mobility of elements by diffusion remains however limited to distances (Figs. 9, 11 and 12) that do not allow a large segregation of elements. Element mobility through convective motion is also restricted to metric scales. Those elements with low values of compatibility are preferentially driven toward the fluid phase.

The intrusion of a new and hotter magma volume also modifies the fluid phase. However, when two magmas have similar or close fluid solubility, the exsolved volume by the cooling magma is easily reincorporated within the warming magma. Thus, intrusion of a felsic magma into a felsic magma chamber does not alter the global volume of H_2O and CO_2. In contrast, the solubility curves for S present an opposite concavity for felsic and mafic magmas (Fig. 2). It results that the largest S content carried by a mafic magma cannot enter into felsic melts at a given ambient pressure. The released fluid thus strongly modifies the composition of the fluid phase. Apparently, halogens (Cl, F, Br) have a similar behavior, and are preferentially hosted in aluminous magmas (Webster, 1997; Boni and Large, 2003).

8.3. Controlling factors for Sn-W ore formation

Identifying all controlling factors leading to Sn-W ore formation seems presumptuous and would signify the end of ore exploration. Nevertheless, some trails appear that result from the succession of magmatic intrusions in a deep magma chamber. This supposes that the hydro-magmatic phase of ore formation is a secondary process, though induced by the magmatic phase. It will not be considered here, though it might represent an important phase, especially for Sn deposits, as observed in Cornwall (Gleeson et al., 2000). It also suggests that the magmatic history of the granitic pluton bears some characters leading to ore formation. This moves the ore formation back to magmatism, and not only to the post-magmatic history

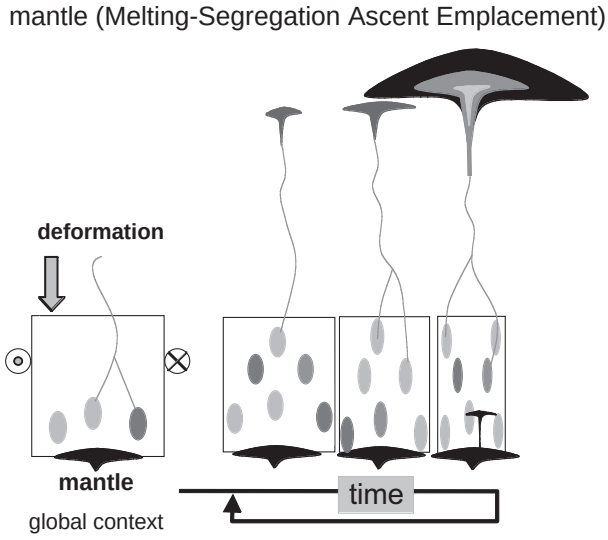

Fig. 15 Granite generation considered as a continuum of discontinuous events from melting to emplacement forming the m(M-SAE) model (Vigneresse, 2004). Melt segregates and starts ascending in the first phases of melting. Emplacement is a suite of discontinuous magma inputs with evolving chemistry, but also with mafic magma inputs. A local stress pattern controls the successive phases of magma generation. The role of the mantle is also necessary as a stress and heat provider.

(Heinrich et al., 2004). This point is important, since it could led to identify what are the magmatic episodes, or what were their successions, that finally result in having barren or mineralized intrusions within the same tectonic settings and time period.

The building of granitic plutons is presently considered as the result of discontinuous events, driven by a continuous melting with help of the underlying mantle (Vigneresse, 2004). This new paradigm has been identified as m(M-SAE) standing for the mantle involvement followed by melting, and a succession of discontinuous segregation, ascent and emplacement (Fig. 15). Numerous field evidences demonstrate the ubiquitous presence of several magma types, more or less assimilated and mixed together (Bergantz, 1995). The present paper was focused on the thermal perturbations induced by those successive intrusions. As dedicated to Sn-W ore deposits, it also only considered those crustal-derived magmas, generally reduced, rich in fluids and emplaced at depth (Fig. 1).

In those conditions, several points merit attention.

- First, the initial magma is a melt that may be considered as a solution in which ions or polymers present weaker bounds than those existing in crystalline arrangements.
- Second, this melt is not very mobile, or mobile as a whole, but without large scale internal convection. This results from the small volumes of magma successively segregated and delivered to the magma chamber. It profoundly differs from a unique magmatic body, about 5

km in radius, of low viscous melt, that could convect entirely (Brandeis and Jaupart, 1986). Sufficient is the absence of evidences in the field for large convection, as well as the difficulty for a low viscous reservoir to maintain ambient stresses in the continental crust.

- Third, the fluid phase associated with the magma seems essential. In particular, the mode of release, through first and second boiling, is specific to each magma type. Magmas giving place to Sn-W porphyry deposits, certainly have a different fluid release history compared to magmas leading to Cu-Mo deposits, generally emplaced higher in the crust. The quantity and nature of the fluid phase are also important. One result of the present work is the evidence of differential S release from mafic and felsic magmas. In contrast, the balance between exsolved and re-dissolved H_2O and CO_2 seems to be of no importance.
- Fourth, the nature of the links between elements in the melt appears to control the final segregation of metals. It seems interesting to address ore formation in terms of electronic structure, looking at M^{4+} sites for metals. Those different metals are often associated, in different amount that depends on the chemico-thermal environment. Hence the presence of M^{4+} metals suggests that they form hard acids because of their high ionic potential. It thus suggests that hard ligands are required, such as Cl^- or F^- to help in transporting metals. Hence, they are the two major anions entering the fluid phase (Webster et al., 1997; Webster, 2004) and halide ligands form stable complexes with metallic cations at all temperatures (Holland, 1972; Helgeson et al., 1978). They are responsible for the transport of many metals in hydrothermal solutions. They should also play a major role in the magmatic phase, i.e. in the melt, of ore deposits (Harris et al., 2003).

9. Conclusions

Successive magma inputs progressively built a large granitic body. The successive magma venues occur with different temperature and chemistry. Owing to those variations in temperature, the yet emplaced magma, as well as the new magma, rapidly re-equilibrate in temperature, thus change their ability of diffusing elements. The new magma cools rapidly, which damps element diffusion. In contrast, heating the former magma enhances element diffusion. A characteristic length is computed, indicating the change induced by the intrusion of the new hot magma. Several cases have been considered, with the simplification of having a granite and a basalt as magma types. Their temperatures of intrusion are fixed at 800 and 1200°C respectively. The temperature of the former magma is selected 200°C below the preceding values. When the two magmas are of similar composition, the change in diffusion length is often less than a factor of five, less than one order of magnitude. The latter is reached when a felsic magma intrudes a mafic magma chamber. The largest effect occurs when a mafic magma at 1200°C enters a yet cold, at 600°C, felsic magma chamber. The diffusion length decreases up to about three orders of magnitude in the basalt whereas it increases of the same amount in the hot mafic magma. The elements with large activation energy, i.e. with the largest ionic radius and large charges, such as Sb, Sn, Zn and Zr, are the most affected. They are sucked from the mafic magma and enrich the felsic one. The present first order model of intrusion emphasizes the role played by successive magma intrusions in the processing of ore formation.

Acknowledgements: This paper came out after a long time spent on granite magmas genesis partly funded by U mining companies and CREGU. It results from an effort to better understand the genesis of ore formation, commonly questioned by academic investigations realized through the CREGU. In this sense, the paper benefited from active support from CREGU. P. Lagrange (CREGU) offered his skill and judicious advices for the illustrations. Numerous judicious comments by one reviewer (Bob Linnen) contributed to improve the reasoning and to clarify some aspects about element partitioning. Encouragements to work on this specific aspect of ore genesis came from Shunso Ishihara and Holly Stein. Both are warmly acknowledged here. Finally the paper is part of the GDR TRANSMET, with aims to describe and identify the processes leading to ore formation.

References

Anderson, O. L. and Stuart, D. A. (1954) Calculation of activation energy of ionic conductivity in silica glasses by classical methods. Jour. Amer. Ceram. Soc., 37, 573–580.

Bea, F. (1996) Controls on the trace element composition of crustal melts. Trans. Royal Soc. Edinburgh Earth Sci., 87, 33–41.

Bea, F., Pereira, M. D. and Stroh, A. (1994) Mineral/leucosome trace-element partitioning in a peraluminous migmatite (a laser ablation-ICP-MS study). Chem. Geol., 117, 291–312.

Behrens, H. and Jantos, N. (2001) The effect of anhydrous composition on water solubility in granitic melts. Amer. Mineral., 86, 14–20.

Bergantz, G. W. (2000) On the dynamics of magma mixing by reintrusion: implications for pluton assembly processes. Jour. Struct. Geol., 22, 1297–1309.

Bingen, B., Demaiffe, D. and Hertogen, J. (1996) Redistribution of rare earth elements, thorium and uranium over accessory minerals in the course of amphibole to granulite facies metamorphism: The role of apatite and monazite in orthogneiss from southern Norway. Geochim. Cosmochim. Acta, 60, 1341–1354.

Blevin, P. L. (2004) Redox and compositional parameters for interpreting the granitoid metallogeny of eastern Australia: Implications for gold-rich ore systems. Resource Geol., 54,

241–252.

Blevin, P. L., Chappell, B. W. and Allen, C. M. (1996) Intrusive metallogenic provinces in eastern Australia based on granite source and composition. Trans. Royal Soc. Edinburgh Earth Sci., 87, 281–290.

Blundy, J. and Wood, J. (2003) Partitioning of trace elements between crystals and melts. Earth Planet. Sci. Lett., 210, 383–397.

Boni, M. and Large, D. (2003) Nonsulfide zinc mineralization in Europe: An overview. Econ. Geol., 98, 715–729.

Bouchez, J. L. (1997) Granite is never isotropic: an introduction to AMS studies of granites. *in* Bouchez, J. L., Hutton, D. H. W. and Stephens, W. E. (eds.) Granite: from Segregation of Melt to Emplacement Fabrics. 95–112, Kluwer Acad. Publ., Dordrecht.

Boyd, F. R. and England, J. L. (1963) Effect of pressure on the melting of diopside, $CaMgSi_2O_6$, and albite, $NaAlSi_3O_8$, in the range up to 50 kilobars. Jour. Geophys. Research, B68, 311–323.

Brady, J. B. (1995) Diffusion data for silicate minerals, glasses and liquids. *in* Mineral Physics and Crystallography: A Handbook of Physical Constants. 269–290, Amer. Geophys. Union Reference Shelf 2.

Brandeis, G. and Jaupart, C. (1986) On the interaction between convection and crystallization in cooling magma chambers. Earth Planet. Sci. Lett., 77, 345–361.

Brandeis, G. and Jaupart, C. (1987) The kinetics of nucleation and crystal growth and scaling laws for magmatic crystallization. Contrib. Mineral. Petrol., 96, 24–34.

Breiter, K., Förster, H. J. and Seltmann, R. (1999) Variscan silicic magmatism and related tin-tungsten mineralization in the Erzgebirge-Slavkosky Les metallogenic province. Mineral. Deposita, 34, 505–521.

Brice, J. C. (1975) Some thermodynamic aspects of the growth of strained crystals. Jour. Crystal Growth, 28, 249–253.

Burdett, J. K. (1995) Structural-electronic relationships in rutile. Acta Crystal., B51, 547–558.

Burg, J. P. and Vigneresse, J. L. (2002) Non-linear feedback loops in the rheology of cooling-crystallising felsic magma and heating-melting felsic rock. *in* Drury, M. (ed.) Deformation Mechanisms, Rheology and Tectonics. Geol. Soc. London, Spec. Publ., 200, 275–292.

Burgisser, A., Bergantz, G. W. and Breidenthal, R. E. (2005) Addressing complexity in laboratory experiments: the scaling of dilute multiphase flows in magmatic systems. Jour. Volcan. Geotherm. Research, 141, 245–265.

Candela, P. A. (1992) Controls on ore metal ratios in granite-related ore systems: an experimental and computational approach. Trans. Royal Soc. Edinburgh Earth Sci., 83, 317–326.

Candela, P. A. and Blevin, P. L. (1995) Do some miarolitic granites preserve evidence of magmatic volatile phase permeability? Econ. Geol., 90, 2310–2316.

Candela, P. A. and Bouton, S. L. (1990) The influence of oxygen fugacity on tungsten and molybdenum partitioning between silicate melts and ilmenite. Econ. Geol., 85, 633–640.

Candela, P. A. and Holland, H. D. (1986) A mass transfer model for copper and molybdenum in magmatic hydrothermal systems; the origin of porphyry-type ore deposits. Econ. Geol., 81, 1–19.

Cann, J. R. (1970) Upward movement of granitic magma. Geol. Mag., 107, 335–340.

Carlslaw, H. S. and Jaeger, J. C. (1959) Conduction of Heat in Solids. Oxford Univ. Press, Oxford, 510p.

Cashman, K. V. (1990) Textural constraints on the kinetics of crystallization of igneous rocks. Rev. Mineral., 24, 259–314.

Castro, A., Moreno-Ventas, I. and de la Rosa, J. D. (1991) H-type (hybrid) granitoids: a proposed revision of the granite-type classification and nomenclature. Earth-Sci. Rev., 31, 237–253.

Cathles, L. M. (1977) An analysis of the cooling of intrusives by ground-water convection which includes boiling. Econ. Geol., 72, 804–826.

Cathles, L. M., Erendi, A. H. J. and Barrie, T. (1997) How long can a hydrothermal system be sustained by a single intrusive event ? Econ. Geol., 92, 766–771.

Cerny, P., Blevin, P. L., Cuney, M. and London, D. (2005) Granite-related ore deposits. Econ. Geol. 100th Anniv. Vol., 337–370.

Cerny, P., Chapman, R., Ferreira, K. and Smeds, S. A. (2004) Geochemistry of oxide minerals of Nb, Ta, Sn, and Sb in the Varutrask granitic pegmatite, Sweden: The case of an "anomalous" columbite-tantalite trend. Amer. Mineral., 89, 505-518.

Chabiron, A., Alyoshin, A. P., Cuney, M., Deloule, E., Golubev, V. N., Velitchkin, V. I. and Poty, B. (2001) Geochemistry of the rhyolitic magmas from the Streltsovka caldera (Transbaikalia, Russia): a melt inclusion study. Chem. Geol., 175, 273–290.

Chappell, B. W., Bryant, C. J., Wyborn, D., White, A. J. R. and Williams, I. S. (1998) High and low-temperature I-type granites. Resource Geol., 48, 225–235.

Chen, Y., Clark, A. H., Farrar, E., Wasteneys, H. A. H. P., Hodgson, M. J. and Bromley, A. V. (1993) Diachronous and independent histories of plutonism and mineralisation in the Cornubian Batholith, southwest England. Jour. Geol. Soc. London, 150, 1183–1191.

Chickos, J. S. and Acree, W. E. (2003) Total phase change entropies and enthalpies. An update of their estimation and applications to estimations of amphiphillic fluorocarbon-hydrocarbon molecules. Thermochim. Acta, 395, 59–113.

Clarke, D. B. and Clarke, G. K. C. (1998) Layered granodiorites at Chebucto Head, South Mountain batholith, Nova Scotia. Jour. Struct. Geol., 20 1305–1324.

Clemens, J. D. (1990) The granulite – granite connexion. *in* Vielzeuf, D. and Vidal, P. (eds.) Granulite and Crustal Evolution. 25–36, Kluwer Acad. Publ. Dordrecht, NATO ASI ser. C311.

Clemens, J. D. and Petford, N. (1999) Granitic melt viscosity and silicic magma dynamics in contrasting tectonic settings. Jour. Geol. Soc. London, 156, 1057–1060.

Clemente, B., Scaillet, B. and Pichavant, M. (2004) The solubility of sulphur in hydrous rhyolitic melts. Jour. Petrol., 45, 2171–2196.

Cline, J. S. (2003) How to concentrate copper. Science, 302, 2075–2076.

Collins, W. J., Richards, S. R., Healy, B. E. and Ellison, P. I. (2000) Origin of heterogeneous mafic enclaves by two-stage hybridisation in magma conduits (dykes) below and in granitic magma chambers. Trans. Royal Soc. Edinburgh Earth Sci., 91, 27–45.

Crank, J. (1975) The Mathematics of Diffusion. Oxford Univ. Press, Oxford, 414p.

Cuney, M., Marignac, C. and Weisbrod, A. (1992) The Beauvoir topaz-lepidolite albite granite (Massif Central, France): the disseminated magmatic Sn-Li-Ta-Nb-Be mineralization. Econ. Geol., 87, 1766–1794.

Darbyshire, D. P. F. and Shepherd, T. J. (1994) Nd and Sr isotope constraints of the Cornubian batholith, SW England. Jour. Geol. Soc. London, 151, 795–802.

Dietrich, A., Lehmann, B. and Wallianos, A. (2000) Bulk rock and melt inclusion geochemistry of Bolivian tin porphyry systems. Econ. Geol., 95, 313–326.

Einstein, A. (1906) Eine neue Bestimmung der Molekuldimensionnen. Ann. Phys., 19, 289–306.

Eyert, V., Horny R., Höck, K. H. and Horn, S. (2000) Embedded Peierls instability and the electronic structure of MoO_2. Jour. Phys. Cond. Mat., 12, 4923–4946.

Flinders, J. and Clemens, J. D. (1996) Non-linear dynamics, chaos, complexity and enclaves in granitoid magmas. Trans. Royal Soc. Edinburgh Earth Sci., 87, 217–223.

Förster, H. J., Tischendorf, G., Trumbull, R. B. and Gottesman, B. (1999) Late-collisional granites in the Variscan Erzgebirge, Germany. Jour. Petrol., 40, 1613–1645.

Frank, M. R., Candela, P. A. and Piccoli, P. M. (2003) Alkali exchange equilibria between a silicate melt and coexisting magmatic volatile phase: an experimental study at 800°C and 100 MPa. Geochim. Cosmochim. Acta, 67, 1415–1427.

Frenkel, J. (1946) Kinetic Theory of Liquids. Oxford Univ. Press, Oxford, 544p.

Gilbert, A. S. (1999) Entropy-enthalpy compensation in the fusion of organic molecules: implications for Walden's rule and molecular freedom in the liquid state. Thermochim. Acta, 339, 131–142.

Giordano, D. and Dingwell, D. B. (2003) Viscosity of hydrous Etna basalt: implications for Plinian-style basaltic eruptions. Bull. Volcan., 65, 8–14.

Glazner, A. F., Bartley, J. M., Coleman, D. S., Gray, W. and Taylor, R. Z. (2004) Are plutons assembled over millions of years by amalgamation from small magma chambers. Geol. Soc. Amer. Today, 14, 4–11.

Gleeson, S. A., Wilkinson, J. J., Stuart, F. M. and Banks, D. A. (2001) The origin and evolution of base metal mineralising brines and hydrothermal fluids, South Cornwall, UK. Geochim. Cosmochim. Acta, 65, 2067–2079.

Guillet, P., Bouchez, J. L. and Vigneresse, J. L. (1985) Le complexe granitique de Plouaret (Bretagne): Mise en évidence structurale et gravimétrique de diapirs emboités. Bull. Soc. Géol. Fr., 8, 503–513.

Haapala, I. (1997) Magmatic and postmagmatic processes in tin-bearing granites: Topaz-bearing leucogranite in the Eurajoki rapakivi granite stock, Finland. Jour. Petrol., 38, 1645–1659.

Halter, W. E., Pettke, T., Heinrich, C. A. and Bothen-Rutishauser, B. (2002) Major to trace elements analysis of melt inclusions by laser-ablation ICP-MS: methods of quantification. Chem. Geol., 183, 63–86.

Hannah, J. L. and Stein, H. J. (2002) Re-Os model for the origin of sulfide deposits in anorthosite-associated intrusive complexes. Econ. Geol., 97, 371–383.

Harris, A. C., Kamenetsky, V. S., White, N. C., Van Achterberg, E. and Ryan, C. G. (2003) Melt inclusions in veins: Linking magmas and porphyry Cu deposits. Science, 302, 2109–2111.

Harris, N., Ayres, M. and Massey, J. (1995) Geochemistry of granitic melts produced during the incongruent melting of muscovite: Implications for the extraction of Himalayan leucogranite magmas. Jour. Geophys. Research, B100, 15767–15777.

Harris, N., Vance, D. and Ayres, M. (2000) From sediment to granites: timescales of anatexis in the upper crust. Chem. Geol., 162, 155–167.

Helgeson, H. C., Delany, J. M. and Nesbitt, H. W. and Bird, D. K. (1978) Summary and critique of thermodynamic properties of rock forming minerals. Amer. Jour. Sci., 278A, 1–299.

Hirschmann, M. M., Asimow, P. D., Ghiorso, M. S. and Stolper, E. M. (1999) Calculation of peridotite partial melting from thermodynamic models of minerals and melts. III. Controls on isobaric melt production and the effect of water on melt production. Jour. Petrol., 40, 831–851.

Hoffmann, A. W. (1980) Diffusion in natural silicate melts: a critical review. *in* Hargraves, R. B. (ed.) Physics of Magmatic Processes. 385–417, Princeton Univ. Press, Princeton.

Holland, H. D. (1972) Granite, solutions and base metal deposits. Econ. Geol., 67, 281–301.

Holtz, F., Johannes, W., Tamic, N. and Behrens, H. (2001) Maximum and minimum water contents in granitic melts generated in the crust: a revaluation and implications. Lithos, 56, 1–14.

Icenhower, J. P. and London, D. (1995) An experimental study of element partitioning among biotite, muscovite and coexisting peraluminous silicic melts at 200 MPa (H_2O). Amer. Mineral., 80, 1229–1251.

Iwamori, H., McKenzie, D. and Takahashi, E. (1995) Melt generation by isentropic mantle upwelling. Earth Planet. Sci. Lett., 134, 253–266.

Jambon, A. (1982) Tracer diffusion in granitic melts: experimental results for Na, K, Rb, Cs, Ca, Sr, Ba, Ce, Eu to 1300°C and a model of calculation. Jour. Geophys. Research, B87, 10797–10810.

Johannes, W. and Holtz, F. (1996) Petrogenesis and Experimental Petrology of Granitic Rocks. Springer, Berlin, 335p.

Keppler, H. and Wyllie, P. J. (1991) Partitioning of Cu, Sn, W, U, and Th between melt and aqueous fluid in the systems haplogranite-H_2O-HCl and haplogranite-H_2O-HF. Contrib. Mineral. Petrol., 109, 139–150.

Knoche, R., Dingwell, D. B. and Webb, S. L. (1992) Non-linear temperature dependence of liquid volumes in the system albite-anorthite-diopside. Contrib. Mineral. Petrol., 111, 61–73.

Koepke, J. and Behrens, H. (2001) Trace element diffusion in andesitic melts: an application of synchrotron X-ray fluorescence analysis. Geochim. Cosmochim. Acta, 65, 1481–

1498.

Kohn, S. C. and Schofield, P. F. (1994) The importance of melt composition in controlling trace-element behaviour: an experimental study of Mn and Zn partitioning between forsterite and silicate melts. Chem. Geol., 117, 73–87.

Kojitani, H. and Akaogi, M. (1997) Melting enthalpies of mantle peridotite: calorimetric determinations in the system CaO-MgO-Al_2O_3-SiO_2 and application to magma generation. Earth Planet. Sci. Lett., 153, 209–222.

Kolker, A. (1982) Mineralogy and geochemistry of Fe-Ti oxide and apatite (nelsonite) deposits and evaluation of the liquid immiscibility hypothesis. Econ. Geol., 77, 1146–1158.

Kovalenko, V. I., Tsaryeva, G. M., Goreglyad, A. V., Yarmolyuk, V. V., Troitsky, V. A., Hervig, R. L. and Farmer, G. L. (1995) The peralkaline granite-related Khaldzan-Buregtey rare metal (Zr, Nb, REE) deposit, western Mongolia. Econ. Geol., 90, 530–547.

Krieger, I. M. and Dougherty, T. J. (1959) A mechanism for non Newtonian flow in suspensions of rigid spheres. Trans. Soc. Rheol., 3, 137–152.

Lesher, C. E. (1994) Kinetics of Sr and Nd exchange in silicate liquids: Theory and experiments, and applications to uphill diffusion, isotopic equilibration and irreversible mixing of magmas. Jour. Geophys. Research, B99, 9585–9604.

Linnen, R. L. (1998) The solubility of Nb–Ta–Zr–Hf–W in granitic melts with Li and Li + F: constraints for mineralisation in rare metal granites and pegmatites. Econ. Geol., 93, 1013–1025.

Linnen, R. L. (2005) The effect of water on accessory phase solubility in subaluminous and peralkaline granitic melts. Lithos, 80, 267–280.

Linnen, R. L. and Keppler, H. (1997) Columbite solubility in granitic melts: consequences for the enrichment and fractionation of Nb and Ta in the Earth's crust. Contrib. Mineral. Petrol., 128, 213–227.

Linnen, R. L., Pichavant, M. and Holtz, F. (1996) The combined effects of f_{O_2} and melt composition on SnO_2 solubility and tin diffusivity in haplogranitic melts. Geochim. Cosmochim. Acta, 60, 4965–4976.

Maaløe, S. (1985) Principles of Igneous Petrology. Springer-Verlag, Heidelberg, 374p.

Magaritz, M. and Hofmann, A. W. (1978) Diffusion of Sr, Ba and Na in obsidian. Geochim. Cosmochim. Acta, 42, 595–605.

Marsh, B. D. (1989) On convective style and vigor in sheet-like magma bodies. Jour. Petrol., 30, 479–530.

McDade, P., Bludy, J. D. and Wood, B. J. (2003) Trace element partitioning on the Tinaquillo lherzolite solidus at 1.5 GPa. Phys. Earth Planet. Int., 139, 129–147.

Mehnert, K. R. (1968) Migmatites and the Origin of Granitic Rocks. Elsevier, Amsterdam, 393p.

Migdisov, A. A. and Williams-Jones, A. E. (2005) An experimental study of cassiterite solubility in HCl-bearing water vapour at temperatures up to 350 °C. Implications for tin ore formation. Chem. Geol., 217, 29–40.

Miller, C. F., Meschter McDowell, S. and Mapes, R. W. (2003) Hot and cold granites? Implications of zircon saturation temperatures and preservation of inheritance. Geology, 31, 529–532.

Mourtada-Bonnefoi, C. C., Provost, A. and Albarède, F. (1999) Thermochemical dynamics of magma chambers: A simple model. Jour. Geophys. Research, B104, 7103–7115.

Müller, A., Breiter, K., Seltman, R. and Pecskay, Z. (2005) Quartz and feldspar zoning in the eastern Erzgebirge volcano-plutonic complex (Germany, Czech Republic): evidence of multiple magma mixing. Lithos, 80, 201–227.

Mungall, J. E. and Dingwell, D. B. (1997) Actinide diffusion in a haplogranitic melt: Effects of temperature, water content and pressure. Geochim. Cosmochim. Acta, 61, 2237–2246.

Mungall, J. E., Romano, C. and Dingwell, D. B. (1998) Multicomponent diffusion in the molten system K_2O-Na_2O-Al_2O_3-SiO_2-H_2O. Amer. Mineral., 83, 685–699.

Mungall, J. E., Dingwell, D. B. and Chaussidon, M. (1999) Chemical diffusivities of 18 trace elements in granitoid melts. Geochim. Cosmochim. Acta, 63, 2599–2610.

Mysen, B. (1998) Transport and configurational properties of silicate melts: relationship to melt structure at magmatic temperatures. Phys. Earth Planet. Int. 107, 23–32.

Navrotsky, A. (1990) Calorimetry of phase transition and melting in silicates. Thermochim. Acta, 163, 13–24.

Patiño Douce, A. E. and Beard, J. S. (1995) Dehydration melting of biotite gneiss and quartz amphibolite from 3 to 15 kbar. Jour. Petrol., 96, 707–738.

Patiño Douce, A. E. and Harris, N. (1998) Experimental constraints on Himalayan anatexis. Jour. Petrol., 39, 689–710.

Patiño Douce, A. E. and Johnston, A. D. (1991) Phase equilibria and melt productivity in the pelitic system: implications for the origin of peraluminous granitoids and aluminous silicates. Contrib. Mineral. Petrol., 107, 202–218.

Petford, N., Cruden, A. R., McCaffrey, K. J. W. and Vigneresse, J. L. (2000) Granite magma formation, transport and emplacement in the Earth's crust. Nature, 408, 669–673.

Pettke, T., Audétat, A., Schaltegger, U. and Heinrich, C. A. (2005) Magmatic-to-hydrothermal crystallization in the W–Sn mineralized Mole Granite (NSW, Australia): Part II: Evolving zircon and thorite trace element chemistry. Chem. Geol., 220, 191–213.

Pitcher, W. S. and Hutton, D. H. W. (1982) Discussion on a tectonic model for the emplacement of the Main Donegal Granite, N. W. Ireland. Jour. Geol. Soc. London, 141, 599–602.

Rabinowicz, M. and Vigneresse, J. L. (2004) Melt segregation under compaction and shear channelling: Application to granitic magma segregation in a continental crust. Jour. Geophys. Research, B109, 10.1029/2002JB002372.

Railsback, L. B. (2003) An earth scientist's periodic table of the elements and their ions. Geology, 31, 737–740.

Raimbault, L., Cuney, M., Azencott, C., Duthou, J. L. and Joron, J. L. (1995) Geochemical evidence for a multistage magmatic genesis of Ta-Sn-Li mineralization in the granite at Beauvoir, French Massif Central. Econ. Geol., 90, 548–576.

Rempel, K. U., Migdisov, A. A. and Williams-Jones, A. E. (2006) The solubility and speciation of molybdenum in water vapour at elevated temperatures and pressures. Implications for ore genesis. Geochim. Cosmochim. Acta, 70, 687–696.

Richardson, S. W. and Oxburgh, E. R. (1978) Heat flow, radiogenic heat production and crustal temperatures in England and Wales. Jour. Geol. Soc. London, 135, 323–337.

Richet, P. and Bottinga, Y. (1984) Anorthite, andesine, wollastonite, diopside, cordierite and pyrope: thermodynamics of melting, glass transitions and properties of the amorphous phases. Earth Planet. Sci. Lett., 67, 415–432.

Richet, P. and Bottinga, Y. (1986) Thermochemical properties of silicate glasses and liquids: a review. Rev. Geophys., 24, 1–25.

Richet, P. and Fiquet, G. (1991) High temperature heat capacities and premelting of minerals in the system MgO-CaO-Al_2O_3-SiO_2. Jour. Geophys. Research, B96, 445–456.

Roberts, M. P. and Clemens, J. D. (1995) Feasibility of AFC models for the petrogenesis of calc-alkaline magma series. Contrib. Mineral. Petrol., 121, 139–147.

Rollinson, H. R. (1993) Using Geochemical Data: Evaluation, Presentation, Interpretation. Longman Group, 352p.

Roscoe, R. (1952) The viscosity of suspensions of rigid spheres. British Jour. Appl. Phys., 3, 267–269.

Rusk, B. G., Reed, M. H., Dilles, J. H., Klemm, L. M. and Heinrich, C. A. (2004) Compositions of magmatic hydrothermal fluids determined by LA-ICP-MS of fluid inclusions from the porphyry copper-molybdenum deposit at Butte, MT. Chem. Geol., 210, 173–199.

Sawka, W. N. (1988) REE and trace element variations in accessory minerals and hornblende from the strongly zoned McMurry Meadows pluton, California. Trans. Royal Soc. Edinburgh Earth Sci., 79, 157–168.

Schaltegger, S., Pettke, T., Audétat, A., Reusser, E. and Heinrich, C. A. (2005) Magmatic-to-hydrothermal crystallization in the W–Sn mineralized Mole Granite (NSW, Australia): Part I: Crystallization of zircon and REE-phosphates over three million years - a geochemical and U–Pb geochronological study. Chem. Geol., 220, 215–235.

Seltmann, R. and Farragher, A. E. (1994) Collisional orogens and their related metallogeny: a preface. *in* Seltmann, R., Kämpf, H. and Möller, P. (eds.) Metallogeny of Collisional Orogens. 7–19, Czech Geol. Surv., Prague.

Shannon, R. D. (1976) Revised effective ionic radii and systematic studies of interatomic distances in halides and chalcogenides. Acta Crystal., A32, 751–767.

Shannon, R. D. and Prewitt, C. T. (1970) Revised values of effective ionic radii. Acta Crystal., B26, 1046–1048.

Shaw, E. and Flood, R. (1981) The New England Batholith, Eastern Australia: geochemical variations in time and space. Jour. Geophys. Research, B86, 10530–10544.

Shinohara, H. and Hendenquist, J. W. (1997) Constraints on magma degassing beneath the Far Southeast porphyry Cu-Au deposit, Philippines. Jour. Petrol., 38, 1741–1752.

Shinohara, H. and Kazahaya, K. (1995). Degassing processes related to magma-chamber crystallization. *in* Thompson, J. F. H. (ed.) Magmas, Fluids and Ore Deposits. Mineral. Assoc. Canada Short Course, 23, 47–70.

Snyder, D. (2000) Thermal effects of the intrusion of basaltic magma into a more silicic magma chamber and implication for eruption triggering. Earth Planet. Sci. Lett., 175, 257–273.

Snyder, D., Crambes, C., Tait, S. and Wiebe, R. A. (1997) Magma mingling in dikes and sills. Jour. Geol., 105, 75–86.

Snyder, D. C., Widom, E., Pietruszka, A. J. and Carlson, R. W. (2004) The role of open-system processes in the development of silicic magma chambers: a chemical and isotopic investigation of the Fogo A trachyte deposit, São Miguel, Azores. Jour. Petrol., 45, 723–738.

Spera, F. J. and Bohrson, W. A. (2001) Energy-constrained open-system magmatic processes I: General model and energy-constrained assimilation and fractional crystallization (EC-AFC) formulation. Jour. Petrol., 42, 999–1018.

Spohn, T., Hort, M. and Fischer, H. (1988) Nucleation simulation of the crystallization of multicomponent melts in thin dikes or sills. I. The liquidus phase. Jour. Geophys. Research, B93, 4880–4894.

Stein, H. J., Markey, R. J., Morgan, J. W., Hannah, J. L. and Schersten, A. (2001) The remarkable Re-Os chronometer in molybdenite: how and why it works. Terra Nova, 13, 479–486.

Stemprok, M. (1993) Genetic models for metallogenic specialization of tin and tungsten deposits associated with the Krusne Hory –Erzgebirge granite batholith. Resource Geol. Spec. Issue, 15, 373–383.

Thomas, R. and Klemm, W. (1997) Microthermometric study of silicate melt inclusions in Variscan granites from SE Germany: Volatile contents and entrapment conditions. Jour. Petrol., 38, 1753–1765.

Thompson, A. B. (1982) Dehydration melting of pelitic rocks and the generation of H_2O-undersaturated granitic liquids. Amer. Jour. Sci., 282, 1567–1595.

Thompson, J. F. H., Sillitoe, R. H., Baker, T., Lang, J. R. and Mortensen, J. K. (1999) Intrusion-related gold deposits associated with tungsten-tin provinces. Mineral. Deposita, 34, 323–334.

Tischendorf, G. (1988) On the genesis of tin deposits related to granites: The example Erzgebirge. Zeits. Geol. Wiss., 16, 407–420.

Turcotte, D. L. and Schubert, G. (1982) Geodynamics. Applications of Continuum Physics to Geological Problems. John Wiley and Sons, New York, 450p.

Vigneresse, J. L. (2004) Toward a new paradigm for granite generation. Trans. Royal Soc. Edinburgh Earth Sci., 95, 11–22.

Vigneresse, J. L. and Améglio, L. (1999) Onset of rigidity during cooling and crystallization of felsic magma intrusions. EUG10 Strasbourg. Jour. Conf. Abstr., 4, 615.

Vigneresse, J. L. and Burg, J. P. (2004) Some insights on the rheology of partially molten rocks. *in* Grocott, J., Tikoff, B., McCaffrey, K. J. W. and Taylor, G. (eds.) Vertical Coupling and Decoupling in the Lithosphere. Geol. Soc. London Spec. Publ. 272, 327–336.

Vigneresse, J. L., Barbey, P. and Cuney, M. (1996) Rheological transitions during partial melting and crystallisation with application to felsic magma segregation and transfer. Jour. Petrol., 37, 1579–1600.

Wada, H., Harayama, S. and Yamaguchi, Y. (2004) Mafic enclaves densely concentrated in the upper part of a vertically zoned felsic magma chamber, The Kurobegawa granitic pluton, Hida Mountain range, central Japan. Geol. Soc. Amer. Bull., 116, 788–801.

Wallace, P. J. (2001) Volcanic SO_2 emissions and the abundance and distribution of exsolved gas in magma bodies. Jour. Volcan. Geotherm. Research, 105, 85–106.

Wallace, P. J. (2005) Volatiles in subduction zone magmas: concentration and fluxes based on melt inclusion and volcanic gas data. Jour. Volcan. Geotherm. Research, 140, 217–240.

Webster, J. D. (2204) The exsolution of magmatic hydrosaline chloride liquids. Chem. Geol., 210, 33–48.

Webster, J. D., Thomas, R., Rhede, D., Förster, H. J. and Seltmann, R. (1997) Melt inclusions in quartz from an evolved peraluminous pegmatite: Geochemical evidence for strong tin enrichment in fluorine-rich and phosphorus-rich residual liquids. Geochim. Cosmochim. Acta, 61, 2589–2604.

Webster, J. D., Thomas, R., Förster, H. J., Seltmann, R. and Tappen, C. (2004) Geochemical evolution of halogen-enriched granite magmas and mineralizing fluids of the Zinnwald tin-tungsten mining district, Erzgebirge, Germany. Mineral. Deposita, 39, 452–472.

Weinberg, R. F. (1999) Mesoscale pervasive felsic magma migration: alternative to dyking. Lithos, 46, 393–410.

Weinberg, R. F. and Leitch, A. M. (1998) Mingling in mafic magma chambers replenished by light felsic inputs: fluid dynamic experiments. Earth Planet. Sci. Lett., 157, 41–56.

Weinberg, R. F., Sial, A. N. and Pessoa, R. R. (2001) Magma flow within the Tavares pluton, northeast Brazil: Compositional and thermal convection. Geol. Soc. Amer. Bull., 113, 508–520.

Whitney, J. A. (1990) Origin and evolution of silicic magmas. Rev. Econ. Geol., 4, 183–201.

Wiebe, R. A. and Collins, W. J. (1998) Depositional features and stratigraphic sections in granitic plutons: implications for the emplacement and crystallization of granitic magma. Jour. Struct. Geol., 20, 1273–1289.

Williams-Jones, A. E., Migdisov, A. A., Archibald, S. M. and Xiao, Z. (2002) Vapour-transport of ore metals. *in* Hellmann, R. and Wood, S. A. (eds.) Water-Rock Interaction, Ore Deposits and Environmental Geochemistry: A Tribute to David A. Crerar. Geochem. Soc. Spec. Publ., 7, 279–305.

Winchell, P. (1969) The compensation law for diffusion in silicates. High Temp. Sci., 1, 200–215.

Wood, B. J. and Blundy, J. D. (1997) A predictive model for rare earth element partitioning between clinopyroxene and anhydrous silicate melt. Contrib. Mineral. Petrol., 129, 166–181.